21.5 CONTAINMENT AND BIMAC PERFORMANCE AGAINST BASEMAT MELT PENETRATION (BMP)

21.5.1 Overall considerations

For all currently operated LWRs, the severe accident management case is based on the so-called core-on-the-floor concept. The basic premise is that, provided there is sufficient floor area available for spreading and sufficient amount of water to cover the molten core debris, the debris will become quenched, and will remain coolable thereafter. Unfortunately, despite extensive commitment of resources, and rather protracted R&D efforts internationally, this idea remains little more than a speculation. While work appears to be continuing, operation of reactors is justified on the basis of analyses that are claimed to satisfy the so-called 24-hour rule. These analyses assume a split of decay power between the upwards (into water) and downwards (into concrete) directions, and predict that (a) basemat penetration will not occur for a minimum of 24 hours, and (b) containment will not fail by accumulation of so-generated non-condensable gases also for a minimum of 24 hours.

While ESBWR satisfies the basic conditions for this approach as intended, with a LDW floor area according to the EPRI URD guidelines for advanced reactors, and while our analyses, such as those described above, show that the 24-hour rule is satisfied with great margins (more than 72 hours), this core-on-the-floor approach was not considered appropriate here. Rather we have incorporated hardware and procedures that make the issue of corium-concrete interactions, along with the great uncertainties that arise in its consideration, mute.

The importance of assuring long term coolability has been also appreciated by other designers of advanced passive plants: the AP600 was provided with features that assure in-vessel retention and coolability, the AP1000 has followed the same approach, and the European Pressurized Reactor (EPR) design placed this line of defense ex-vessel, by means of a rather elaborate scheme for facilitating corium spreading and heat removal (Fisher, 2003). Further, the new Russian V-320 design of VVER1000 plant (under construction in Tianwan, China) has a very elaborate ex-vessel core catcher, which includes a basket made of Al_2O_3-Fe_2O_3-steel mixture and filled with a special material compound (Kukhtevich, 2001).

21.5.2 ESBWR Design

Inspired by, and leveraging on IVR technology developed during DOE's ARSAP program nearly a decade ago (Theofanous et al, 1996), we employ here a passively cooled boundary that is impenetrable by the core debris in whatever configuration it could possibly exist on the LDW floor. For ex-vessel implementation this boundary is conveniently, and advantageously made by a series of side-by-side placed inclined pipes, forming a jacket which can be effectively and passively cooled by natural circulation when subjected to thermal loading on any portion(s) of it. Water is supplied to this device from the GDCS pools via a set of deluge lines (we call these the LDW deluge lines). The timing and flows are such that (a) cooling becomes available immediately upon actuation, and (b) the chance of flooding prematurely the LDW to an extent that opens up a vulnerability to steam explosions is very remote. The detection/activation system will be finalized at the COL stage the design, and the required unreliability (at a high confidence level) of it is now specified to 10^{-3} per demand. The jacket is buried inside the concrete basemat and would be called into action immediately upon the first melt arrival on the LDW floor.

The device, called Basemat Internal Melt Arrest and Coolability device (BiMAC) (Theofanous and Dinh, 2005), is illustrated in Figure 21.5.2-1. Important considerations in the design and implementation of this concept are as follows:

a. **Pipe inclination angle**. As we show further below, both the thermal load due to melt natural circulation (q_D), and the burnout heat flux (the CHF), increase with angle of inclination of the bottom boundary from a low value pertinent to a near horizontal orientation. This increase is much faster for the CHF in the region $0<\theta<20^0$, and there is a maximum separation from q_D at around the upper end of this range. Within a reasonable value of the overall vertical dimension of the BiMAC device, the whole LDW can be covered conveniently with pipes inclined at near the upper end of this range.

b. **Sacrificial refractory layer.** A refractory material is laid on top of the BiMAC pipes so as to protect against melt impingement during the initial (main) relocation event, and to allow some adequately short time for diagnosing that conditions are appropriate for flooding. This is to minimize the chance of inadvertent, early flooding. The material is selected to have high structural integrity, and high resistance to melting — such as is for ceramic Zirconia. As shown below, with this material, a layer thickness of 0.2 m (8 in) is quite adequate to meet these design objectives. Final design details of the BiMAC will be consistent with Reference 21.5-40.

c. **Cover plate.** As shown in Figure 21.5.2-1, we use a supported steel plate to cover the BiMAC. On the one hand this allows that the top is a floor as needed for normal operations, and that the BiMAC is basically "out of the way" until its function is needed. On the other hand the so-created cavity, with a total capacity of ~90 m^3 (3200 ft^3), is there to receive and trap all possible quantity of melt in a hypothetical ex-vessel severe accident evolution, including a high pressure melt ejection (see Section 21.3). For this purpose the top plate is stainless steel, 2 mm (0.08 in) in thickness so as to be essentially instantaneously penetrable by a high-velocity melt jet. The plate is made to sit on top of normal floor grating, which itself is supported from below by steel columns as indicated schematically in the same figure. (Further details on this simple support system are straightforward engineering tasks more pertinent to the COL stage of the plant design and review). Between the plate and the grating we have a layer of refractory material, like a mat of zirconium oxide, so as to protect the steel material from thermal loads from below during the ~ 40 s needed to the end of steam blowdown, yet not able to provide any structural resistance to melt penetration as needed for the trapping function noted above. For low pressure sequences, this whole cover structure has no bearing on the outcome.

d. **The BiMAC cavity.** The space available below the BiMAC plate is sufficient to accommodate the full-core debris, while the whole space available, up to a height of the vertical segments of the BiMAC pipes, amounts to a volume of ~400% of the full-core debris. Thus there is no possibility for the melt to remain in contact with the LDW liner. Similarly, the two sumps, needed for detecting leakage flow during normal operation, are positioned and protected in the same manner as is the rest of the LDW liner (Figure 21.5.2-1d). There is complete floor coverage.

e. **The LDW deluge system.** According to the preliminary design, this system consists of three main lines that feed off the three GDCS pools, respectively, each then separating into a pair of lines. One from each pair of these lines connects to the BiMAC main header, the other discharges directly into the LDW from near the top (Figure 21.5.2-1). There are six valves, one for each line. Three of them (the ones that feed into the BiMAC) are operated off numerous thermocouples/conductivity probes that cover the LDW floor area to a sufficient degree to indicate melt arrival following RPV breach. The other three, the ones that fed directly into the LDW, will be designed to provide a diverse detection and activation system. The lines are sized so that any three of them would be sufficient to ensure proper BiMAC functioning; that is capable to operate in the natural circulation mode within 5 minutes from melt arrival on the floor. As noted above the required failure rate of the system (at high confidence) is not to exceed 10^{-3} per demand. [As shown in DCD Tier 2 Chapter 6 Figure 6.3-1, there are 4 deluge lines coming from the GDCS, each connected to 3 deluge valves. The interface between the deluge lines and BiMAC downcomers and lower drywell deluge will be determined in the detailed design phase.]

As described below, the BiMAC concept is based on fundamental analytical considerations built on top of separate-effects experiences on burnout heat fluxes in inverted geometries, and two-phase (boiling) pressure drop in inclined pipes. These provide reasonable confidence that the concept is sound.

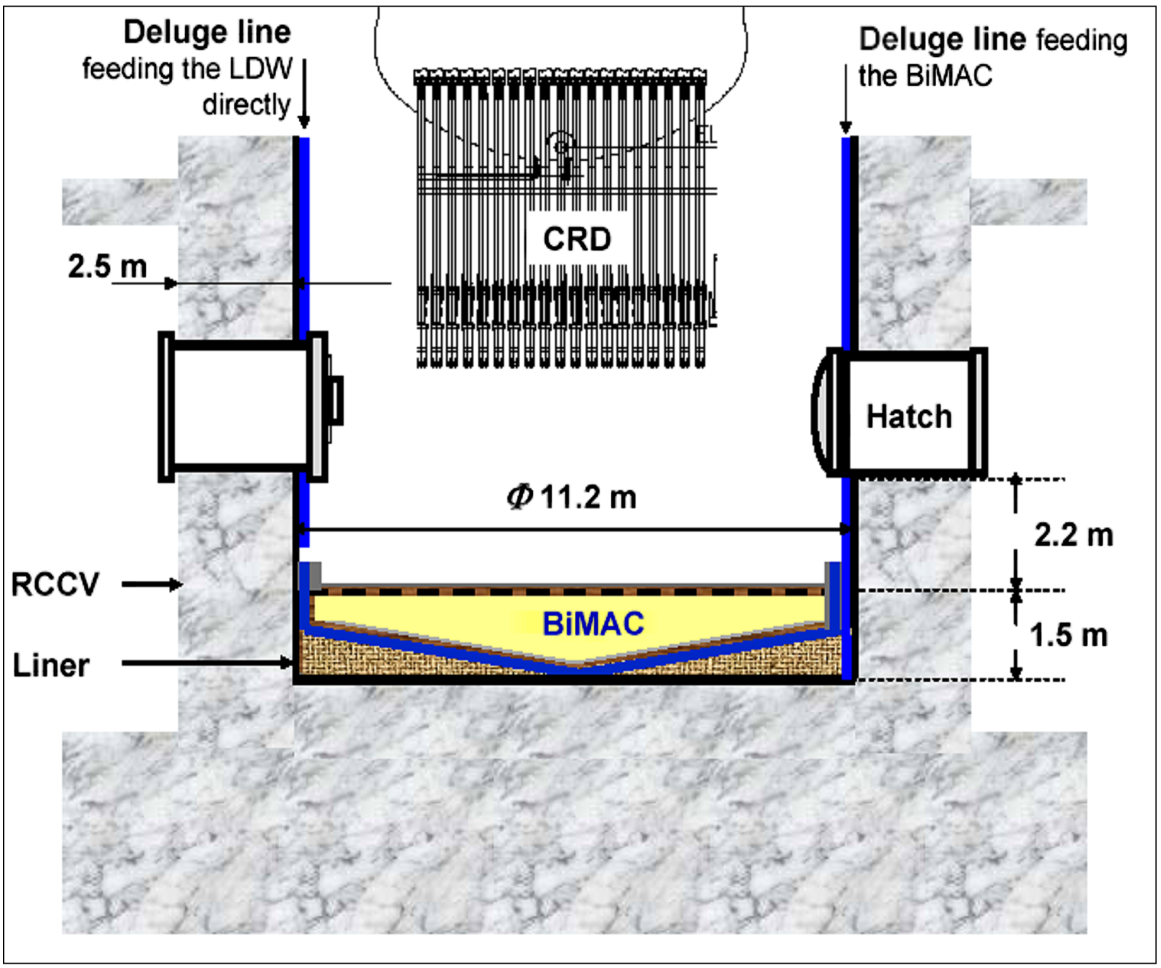

Figure 21.5.2-1a. The BiMAC Positioned Inside the LDW

The BiMAC positioned inside the LDW. Initial cooling is provided by the flow into the BiMAC. The LDW is flooded independently by the direct flow.

ESBWR Design (Addendum of May 7, 2007)

This is in response to Prof. Griffith's request for further clarification of the BiMAC design concept. In addition to Figure 21.1-1 in Section 21.1, Figure 21.5.2.1aa shows the placement of the BiMAC inside the containment. A scaled 3D rendering of the BiMAC basic pipe structure is shown in Figure 21.5.2-1ca (¼ symmetry). As noted throughout details such as angle of inclination, sacrificial material choice, and BiMAC cover (LDW floor), will be optimized on the basis of the BiMAC coolability experiments.

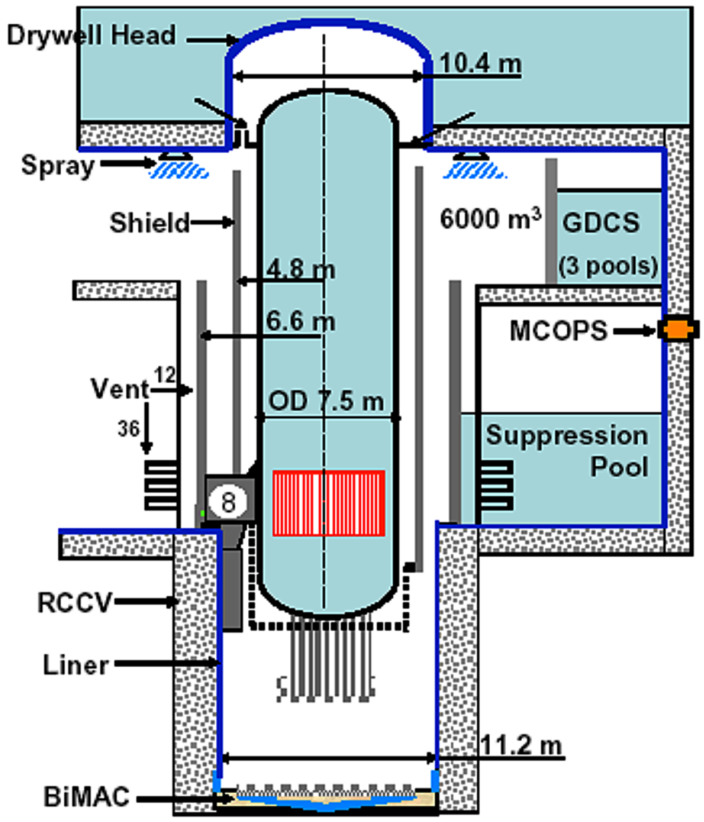

Figure 21.5.2.1aa. Same as Figure 21.5.2-1a but in a different perspective

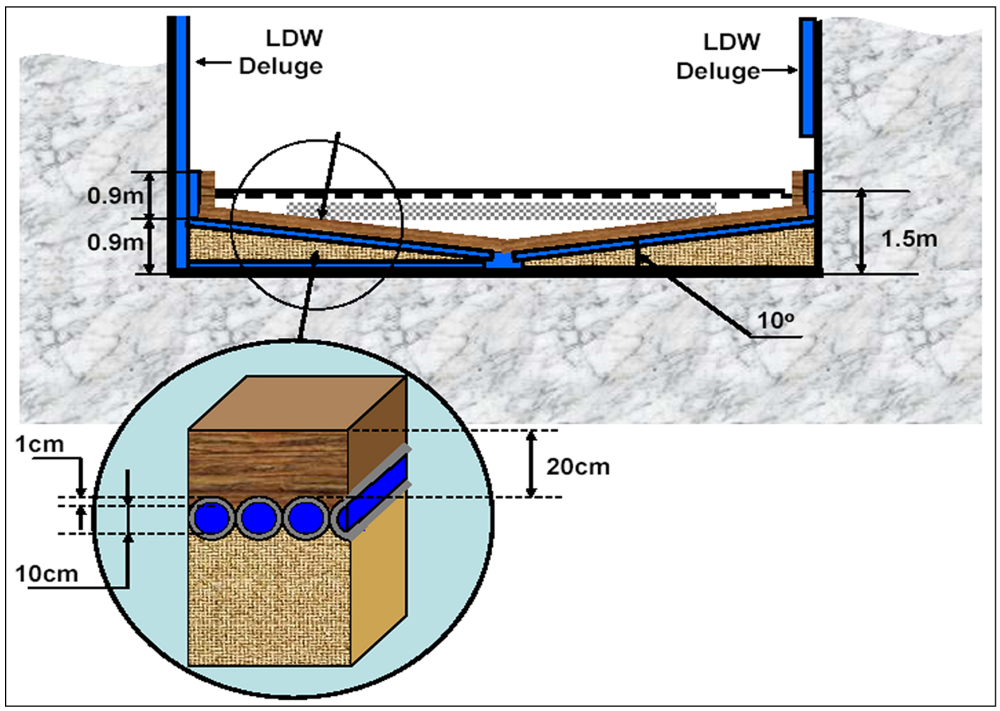

Figure 21.5.2-1b. The BiMAC Pipes and Protective Ceramic Layer
[Final design details of the BiMAC will be consistent with Reference 21.5-40.]

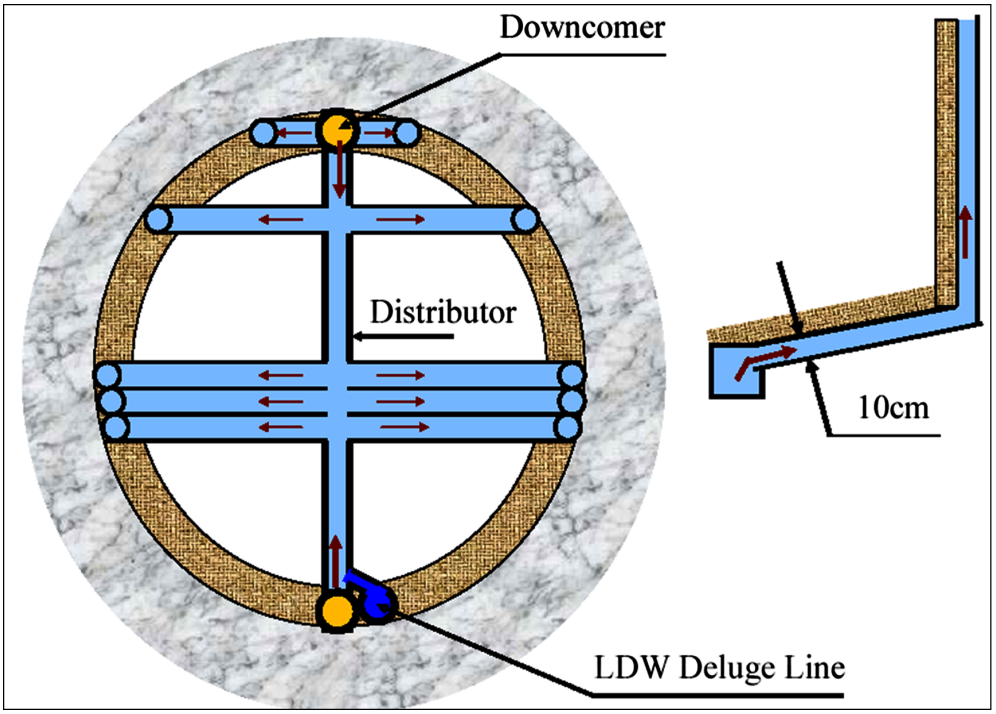

Figure 21.5.2-1c. Schematic Arrangement of the BiMAC Pipes

Schematic arrangement of the BiMAC pipes to form a wedge-shaped jacket. The distributor (the vertical blue line in the figure) serves as the main header. The downcomers (marked in yellow, connected to the distributor) and the pipes, including the vertical segments, serving as risers, form natural circulation loops that respond passively to the local cooling demand.

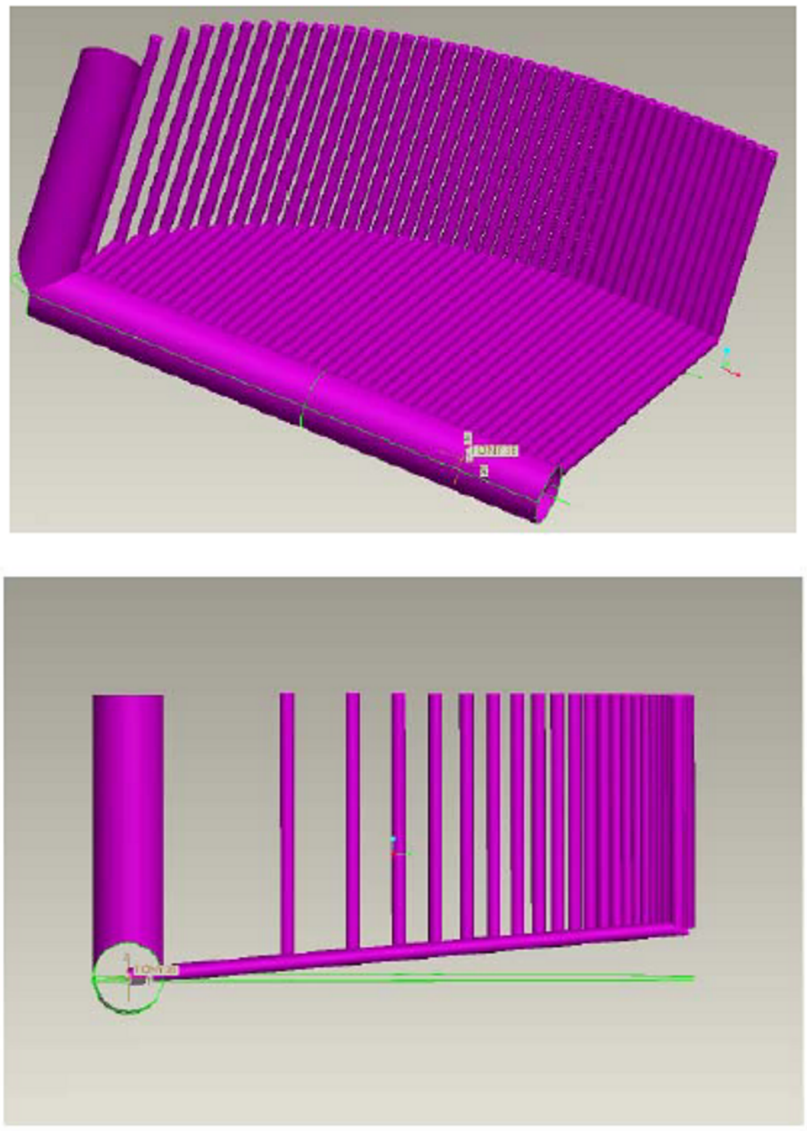

Figure 21.5.2-1ca. A scaled 3d rendering of Figure 21.5.2-1c, in ¼ symmetry

Perspective views of the BiMAC as rendered in the experimental facility design concept. Top: an oblique/down view. Bottom: a diametric/horizontal view. The facility represents an one-quarter equivalent at ½-linear scale.

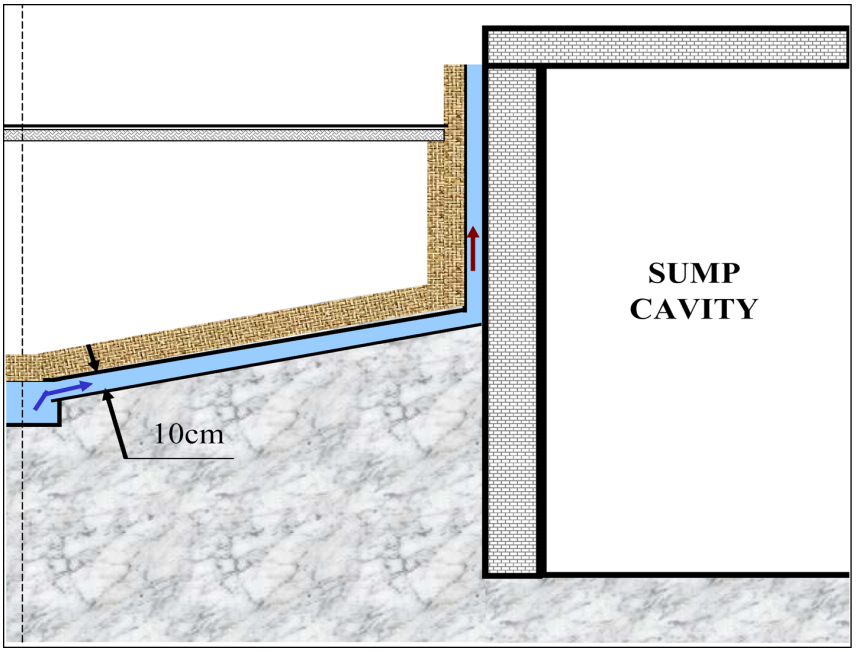

Figure 21.5.2-1d. Schematic Representation of a Sump and Its Protection

Schematic representation of a sump and its protection (against melt attack) by the BiMAC cooling pipes. There are two sumps, shaped and positioned next to the pedestal wall so that they offer no significant "target" to the melt stream exiting the vessel under most release scenarios. [The Drywell LCW (Low Conductivity Waste) Sump will be located above the lower drywell floor.] There is no other place for melt to go except into the BiMAC. Not to scale.

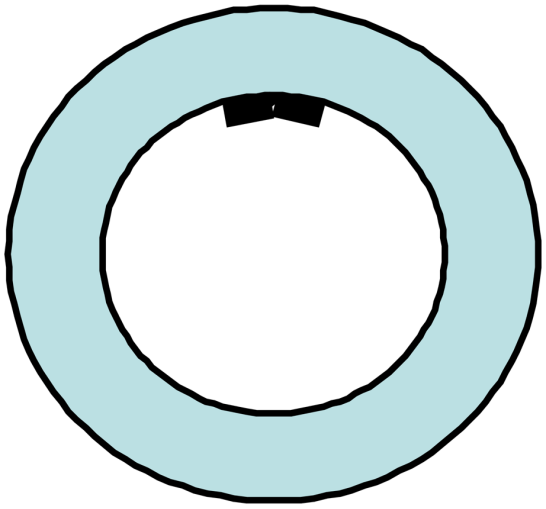

Figure 21.5.2-1e. The Two Sump Positions Inside the Reactor Pedestal

The two sump positions inside the reactor pedestal. Top view, to scale.

21.5.3 Previous Work

As noted already the BiMAC was inspired by the IVR coolability concept, and its design is based on basic technology developed during this earlier work done under DOE's ARSAP program. This technology includes the initial (Configuration I) ULPU tests that quantify CHF as a function of inclination (Theofanous and Syri, 1997), the ACOPO tests that quantify natural convection loads from volumetrically-heated pools (Theofanous and Angelini, 2000), and ROAAM that provides the organizing principle for the whole assessment (Theofanous et al, 1994, 1996). One major simplification at present is that the behavior is not susceptible to the so-called "focusing effect", a phenomenon that can arise in in-vessel situations when (if) there is an insufficient amount of molten steel to spread the heat over a large enough area of the side wall, together with the absence of water on top of the molten pool.

Since this early work, there has been an intense follow-up internationally on IVR, including a CSNI specialist's meeting (Garching, 1994), several test programs in France (SULTAN tests), Finland (COPO tests, VTT tests), Sweden (SIMECO, FOREVER tests), Korea (KAIST tests), and Russia (RASPLAV, MASCA tests). All this work is confirmatory of the work done by UCSB for the Loviisa, AP600 and AP1000.

In addition, and on fundamental grounds, since that time the mechanism of Boiling Crisis is understood better (Theofanous et al., 2002a, 2002b; Theofanous and Dinh, 2002, 2004). So is natural convection (Theofanous and Angelini, 2000; Dinh et al., 2004a, 2004b). The latter has been also greatly impacted by advances in CFD and computing power that allow rather detailed Direct Numerical Simulations (DNS) of such phenomena with great reliability. We make use of this simulation capability for assessing the thermal loads in the present 2D wedge-shaped geometry.

21.5.4 Present Assessment

21.5.4.1 Key Physics

Successful functioning of the BiMAC devise depends crucially on the condition that heat removal capability (by boiling) exceeds the thermal loading due to melt natural convection. Thus, quite simply, the key physics here concern processes that control the magnitude of these two outcomes. In addition, it must be shown that, at the end of the main melt relocation event, and associated ablation process, the BiMAC sacrificial layer is left with some material still protecting the steel pipes, and this needs to be done both for HP as well as for LP sequences.

a. **Thermal Loads.** Any amount of core debris that is not coolable, will form into a molten pool that, heated in volume, and rejecting heat to the outside through all its boundaries, would eventually reach a quasi-steady, maximum extend configuration. This means that such a molten pool would tend to spread, incorporating more and more debris and concrete material, until eventually all heat supplied to all of its boundaries from the inside is removed by conduction through the surrounding solid crusts and associated materials found on the outside. Thus at the top boundary, it being in contact with water, this balance between heat supply and rejection would define the thickness of the solidified material that is assumed to exist, persist, and be impenetrable to water— for otherwise, the debris would be coolable on its own, without a need for BiMAC. At the bottom boundary, the melting would extend eventually to a degree that

only a rather thin layer of remaining sacrificial material and solidified debris would separate the melt from the steel pipes below. Thus, all around on the inside, the molten pool would see the liquidus temperature, while it develops the amount of superheat needed for rejecting the decay power generated within. We are mainly interested on the thermal loads delivered to the lower, wedge-shaped boundary, and to any vertical boundaries for pools that are voluminous enough to create a submergence of the vertical pipe segments. Bounding estimates of these loads can be obtained by assuming a maximum extent pool involving the total amount of core-and-internals debris possible. From previous experience (for example Angelini and Theofanous, 1995) with such large, high Rayleigh number pools, we know that these loads are spatially non-uniform and that the magnitudes increase with angle of inclination of the lower boundary reaching a maximum at vertical boundaries. We also know that a key parameter, the up-to-down power split, is typically in a proportion within the 2 to 3 range. Thus on an average basis we have here, at the most, a downwards heat flux in the ~100 kW/m^2 (8.8 $Btu/s.ft^2$) range, while due to the small angle of inclination we can expect, on fundamental grounds, that at local heat peaking would not exceed ~300 kW/m^2 (26 $Btu/s.ft^2$). On the vertical boundary we can expect as much as 300 kW/m^2 (26 $Btu/s.ft^2$) on the average, which with local peaking would yield ~500 kW/m^2 (44 $Btu/s.ft^2$) near the top. It should be noted that these order of magnitude results are provided here for some initial perspectives—results specific to the present geometry and conditions are presented in Subsection 21.5.4.3.

b. **Limits of Coolability.** These limits are defined by the burnout heat flux, or Critical Heat Flux (CHF), of water boiling on the inside of the inclined, and vertical BiMAC pipes. Previous experience in such geometries (Theofanous and Syri, 1997) shows that the CHF increases rapidly with angle of inclination, and that this increase is most rapid in the 0 to 20^o interval, ranging from 300 kW/m^2 (26 $Btu/s.ft^2$) at the low end to 500 kW/m^2 (44 $Btu/s.ft^2$) at the upper end. More recent fundamental data show that burnout in nucleate boiling occurs due to dryout of extremely thin liquid films (tens of microns in thickness) and that surface wettability plays a key role in this dryout (Theofanous et al, 2002a-b). Engineering surfaces such as those of the steel pipes to be employed here were found to be very resilient to dryout. Still, assessment of CHF for any new situation is a matter of empirical determinations under the appropriate geometry and fluid flow conditions that are representative of the application. This was in particular the case for the AP600 and AP1000 (Theofanous et al, 1996, and Dinh et al, 2003), and this is the approach we take here. In addition, we need to be concerned about flow regimes, pressure drop, and flow stability, especially in regards to temporary dryouts, that could develop into irreversible burnouts.

c. **Sacrificial Material Ablation by Jet Impingement.** Heat transfer and related phase change processes during melt jet impinging on a solid slab have been studied extensively in the past and their mechanisms are well understood today (Theofanous et al., 1996). A key consideration is whether the instantaneous contact temperature between the melt and the substrate is below the freezing point of the melt—if so, crusts form upon contact and the thermal boundary condition is the melt liquidus; in other words melt superheat governs the rate of heat transfer. This, along with the jet velocity and the thermo-physical properties, define the rate of heat transfer. These considerations lead to Zirconia as the material of choice for protecting the BiMAC

pipes from melt impingement. By having a melting range (2950 – 3120 K (4850 - 5160°F)) well above the temperature of any reasonably expected metallic melt, the possibility of ablation is completely eliminated. On the other hand, while this is not the case for oxidic jets, the superheats in this case are by comparison (to metallic melts) rather small, and this together with the low thermal conductivities of such melts limit the ablation rates to such low levels that good protection can be achieved without overburdening the device with an excessively thick protective layer. [Final design details of the BiMAC will be consistent with Reference 21.5-40.]

21.5.4.2 Probabilistic Framework

The framework for the BMP assessment, with BiMAC included in the design, is straightforward (Fig. 21.5.4.2-1), and similar to that of Theofanous et al (1996) developed for IVR. Here too there are thermal and mechanical (EVE) loads to be considered. The EVE threat is addressed in Subsection 21.4. The thermal loads include, as in the IVR case, melt-through by direct jet impingement, and by locally exceeding the burnout heat flux. In addition here we have to be concerned about global mechanisms, such as flow instabilities, that could potentially lead to local dry-outs (due to flow supply deficiencies). As noted above, for the impingement problem we have here the luxury (not available in IVR) of selecting the protective material (a refractory).

More specifically, the following additional remarks can be made:

a. Ablation of the protective ceramic layer needs to be addressed under both LP and HP scenarios. The definition of a local ablation depth as a failure criterion refers to a remaining thickness (after ablation) that would be considered structurally stable, consistently with the manner in which the ablation rate has been determined. This is taken as 50 mm (2 in);

b. The thermal load under melt jet impingement, and any amounts of ablation predicted as a result, is to consider both metallic and oxidic melts, at appropriate levels of superheats, and amounts of material potentially involved in the first, major, pour;

c. The thermal loading, is derived from melt natural convection within the BiMAC boundaries, and it informs both thermal failure modes, but in a different emphasis—for the local burnout we are interested in heat flux peaking, such as it occurs at the edges of the inclined portion of the pipes, while for the dryout, we more interested on overall heated channel behavior as driven by total power levels and numbers of channels involved (Section 21.5.4.3), that is by the average values of heat flux;

d. The local critical heat flux, at such power levels as found here, is due to a mechanism very similar to that in nucleate boiling, but at different length and time scales (Angelini et al, 1997, Theofanous et al, 1998, Theofanous et al 2002a,b).

e. The dryout condition is defined by a liquid content that may be insufficient to maintain wetting (due to the near-horizontal orientation) over the whole heated area of the pipe wall—this can arise from strong evaporation along the channel, or from flow instability that involves temporal depletions of sufficient duration to result in dryout.

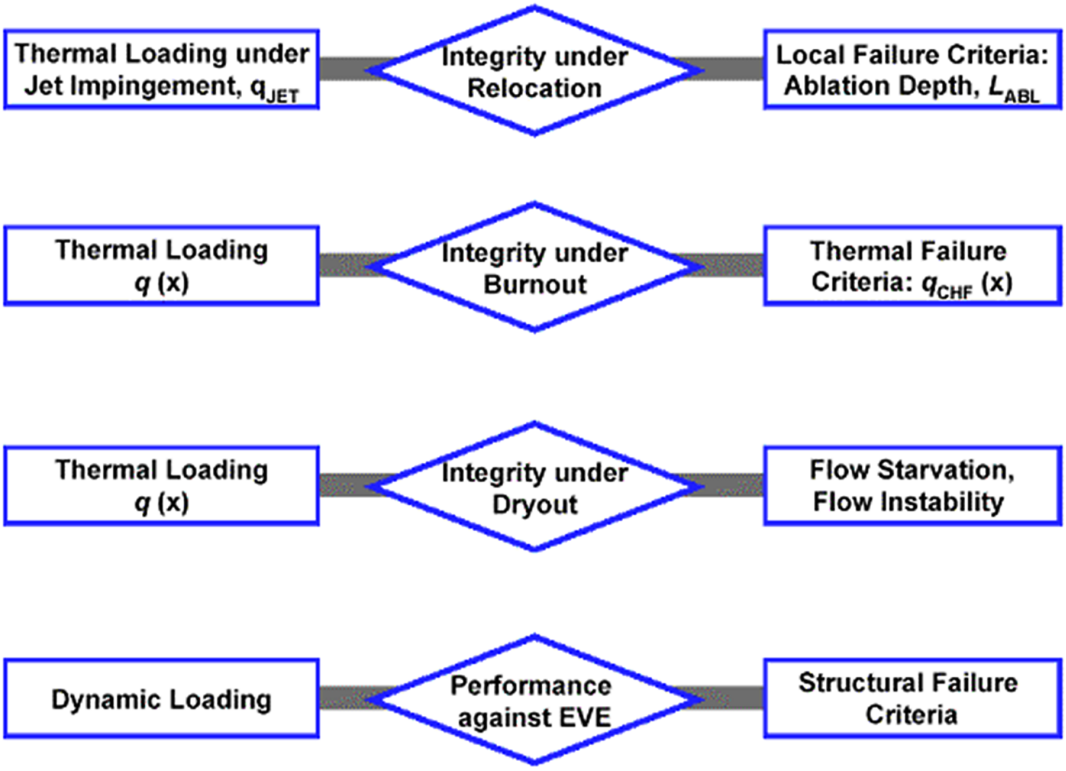

Figure 21.5.4.2-1. The Analysis Scope to Address Failure of Bimac Function

The scope of analysis carried out to address failure of BiMAC function. There are four potential failure modes, as named by the rhombic boxes. In each case we also indicate the applicable loading and failure criteria.

21.5.4.3 Quantification of Loads

Thermal Loads due to Melt Natural Circulation. Thermal loading of the BiMAC can only arise from the portions of corium debris that remain in the molten state and are naturally convecting (heat) to the pool boundaries. These loads will depend on the pool configuration/geometry, and our task here is to bound these loads in a manner that does not depend on the details of vessel breech, melt disposition, and more generally ex-vessel behavior insofar as their effect on pool geometry is concerned. This is a basic requirement, which we feel is appropriate for this stage of accident management.

To begin with we note that:

a. The setting is a fully submerged (in water) debris volume;

b. There is no convecting (metallic) melt layer on top of the oxidic pool—that is absence of the "focusing effects" familiar from the IVR assessments;

c. The initial pour, occurring at the time of lower head breech, would involve some fraction (probably significantly less than 1) of the vessel inventory, and will occur in

essentially dry LDW space, thus spreading to all available space within the BiMAC space;

d. Subsequent discharges will be gradual, and occurring into a flooded LDW, thus being subject to quenching, as they lie on top of the debris found already on the LDW floor, and;

e. A major, if not all, fraction of the core debris that has been quenched, would be coolable, and thus absent from the molten pool energy balance.

In the following, the quantity of the fuel involved in a melt pool will be denoted by the fraction of the total amount possible (220 metric tons (240 tons))—that is, a "50% pool" will be one containing 120 metric tons (130 tons) of molten fuel. The other key variable is decay power density. For simplicity this will be bounded by 1.2 MW/m^3 (32 $Btu/s.ft^3$) (that is, per cubic meter of fuel involved in the melt being considered), which is pertinent to the fastest evolving severe accident sequences in the ESBWR.

An overall view of the melt pool geometries (that is heights and degree to which the vertical boundaries of the BiMAC are submerged) and resulting average heat fluxes (using the 3:1, up-to-down power split discussed above) as functions of the total quantities of melt involved is given in Table 21.5.4.3-1. Clearly the relevant, yet extremely conservative, as explained just above, flux levels are at ~100 kW/m^2 (8.8 $Btu/s.ft^2$) on the lower boundary, and ~300 kW/m^2 (26 $Btu/s.ft^2$) on the side boundary of the BiMAC. These numbers will be used in assessing flow demand and stability requirements of the BiMAC in operation; that is the "Dry-out" question, and this is further pursued in Subsection 21.5.4.4. What remains to be done here is to determine the appropriate peaking factors to apply to these fluxes for the purpose of evaluating the Burnout question. We refer to these as horizontal and vertical peaking, as corresponding to the lower and vertical boundaries respectively.

For this purpose we make use of Computational Fluid Dynamics (CFD) simulations (see Appendix 21D). We considered two pool configurations as defined in Tables 21.5.4.3-2 and 21.5.4.3-3. Configuration I corresponds to a "central" BiMAC channel, that is a slice taken in a near-diametrical position, and melt depths that do not submerge the vertical pipes. Configuration II is chosen to correspond to a near-the-edge channel, that is a slice taken far-off the diametric position, and melt depths that submerge the vertical pipes to levels typical of bounding, full-inventory pools. In order to gain in spatial resolution all these calculations were carried in 2D. The effect of 3D convection was also explored for two conditions: Configuration I case C, and Configuration II case M. The thermo-physical quantities used are summarized in Table 21.5.4.3-4. Key numerical results can be found in Table 21.5.4.3.5. Detailed results are given in Figures 21.5.4.3-1 to 21.5.4.3-5. The following observations can be made on the basis of these results.

a. The 2D calculations yield conservative estimates of the up-to-down power split, as well as for the power peaking along the boundary. This is because in 2D turbulence is artificially restricted thus reducing mixing and turbulent energy transfer down the motion cascade. On this basis we take a split of 3, which is still conservative compared to the calculated value of 3.4. For peaking factors we chose to use, still conservatively, the results from the 2D calculations.

b. Horizontal peaking seems to be insensitive to the pool depth in both configurations. For central channels all cases seem to be well represented by a peaking factor value of 1.25. For near-edge channels the peaking involves a narrow region with sharp rise up to a value of ~3. This is because of the descending, vertical boundary layer (see Figure 21.5.4.3-1b), which creates an "impact" region right around the point where the vertical and near-horizontal boundaries meet.

c. Vertical peaking is rather mild, and it can be well bounded by a value of 1.4.

Applying these results to a full-inventory pool we obtain the following, extremely conservative (bounding) estimates:

For Central Channels:	q_{dn} = 100 W/m^2, (0.0088 Btu/s.ft^2)	$q_{max,dn}$ = 125 W/m^2 (0.011 Btu/s.ft^2)
For Near-Edge Channels:	qdn = 100 W/m2 (0.0088 Btu/s.ft2),	qmaxdn = 300 W/m2 (0.026 Btu/s.ft2)
	q_v = 320 W/m^2 (0.028 Btu/s.ft^2),	$q_{max.v}$ = 450 W/m^2 (0.040 Btu/s.ft^2)

Quantification of thermal loads (Addendum of July 31, 2006)

Due to the importance of the up-to-down power split in the maximum thermal loading estimate of BiMAC, additional calculations were made both in 2D and 3D, with refined nodalization (roughly a reduction of node size by a factor of 4) as indicated in Table 21.5.4.3.5Add. The numbers in parenthesis are the previous results as presented originally in Table 21.5.4.3-5. In addition we explored the effects of increasing the Prandtl number, and decreasing the Rayleigh number due to assumed variations in transport properties. All these variations were made on test case M, considering a central "slice" of the melt pool, 0.1 m in thickness (see Figure 21.5.4.3-2), with periodic or symmetry (zero gradient) boundary conditions on the side-surfaces of this slice.

As seen in Table 21.5.4.3.5Add, the effects of all these variations are minimal, and the results confirm that the value of flux ratio used in our assessment is appropriate, and robustly conservative.

The flux distributions are also consistent with our previous results, except for showing in somewhat accentuated degree (by ~20%) the highly localized corner-region heat flux increases discussed previously in Section 21.5.4.3. As we noted therein, these are somewhat of an artifice of the numerical simulations that do not take into account the effect of crusts at the pool boundaries.

Table 21.5.4.3.5 Add.
Summary of power split results

in refined-grid calculations of melt natural convection in a central BiMAC "slice". The numbers in parenthesis are previous results found in Table 21.5.4.3-5.

Case No.	***RA'***	***Pr***	q_{up}/q_{dn}	***Minimum Node size*** Δx- Δy- Δz ***mm (in)***
M-2D-FG	*1.82 10^{14}*	*0.75*	***2.1*** *(2.0)*	*1-0.5(0.04-0.02)*
M-3D-FG	*1.82 10^{14}*	*0.75*	***3.3*** *(3.4)*	*1-0.5-2 (0.04-0.02-0.08)*
M-3D-FG-Pr	*1.82 10^{14}*	*7.5*	***3.42***	*1-0.5-2 (0.04-0.02-0.08)*
M-3D-FG-Vi	*1.82 10^{13}*	*0.75*	***3.61***	*1-0.5-2 (0.04-0.02-0.08)*

Table 21.5.4.3-1
BiMAC Capacity

BiMAC Capacity as a Function of Melt Pool Height, and Resulting Average Heat Fluxes.
Total Decay Power taken at ~6 Hours into the Accident (36.4 MW)

H_melt, m (in)	**0.2 (8)**	**0.4 (16)**	**0.6 (24)**	**0.8 (32)**	**1.0 (40)**
V_melt[a], m^3 (ft^3)	2.2 (78)	9.(320)	20.5 (724)	35.8 (1260)	53.8 (1900)
Mass, metric tons (tons)	18 (20)	72.5 (79.9)	164 (181)	287 (316)	431 (475)
i_vertical[b]	51	47	41	29	1
V_sump, m^3 (ft^3)	0.3 (11)	0.85 (30)	1.4 (49)	2 (71)	2.6 (92)
M_sacrificial layer, metric tons (tons)	7.6 (8.4)	15 (17)	21.7 (23.9)	27.3 (30.1)	30.7 (33.8)
Top Boundary, m^2 (ft^2)	25 (269)	49 (527)	70.5 (759)	87.7 (944)	95.8 (1030)
Bottom Boundary, m^2 (ft^2)	25.4 (273)	49.7 (535)	71.5 (770)	88 (947)	97.3 (1050)
Side Boundary, m^2 (ft^2)	0	~0	0.8 (8.6)	2.1 (23)	5.1 (55)
	All melt assumed to be Fuel			All oxides + 20 tons of metal	All oxides + 160 tons of metal
Decay power, MW (Btu/s)	1.5 (1400)	8.6 (8200)	21.5 (20,400)	36.4 (34,500)	36.4 (34,500)
Upward heat flux, kW/m^2 ($Btu/s.ft^2$)	45 (4.0)	132 (11.6)	226 (19.9)	305 (26.9)	271 (23.9)
Downward heat flux, kW/m^2 ($Btu/s.ft^2$)	15 (1.3)	43 (3.8)	74 (6.5)	100 (8.8)	89 (7.8)

Table 21.5.4.3-1
BiMAC Capacity

BiMAC Capacity as a Function of Melt Pool Height, and Resulting Average Heat Fluxes.
Total Decay Power taken at ~6 Hours into the Accident (36.4 MW)

Sideward heat flux, kW/m^2 ($Btu/s.ft^2$)	-	-	300 (26)	320 (28)	350 (31)

Notes

a. V_melt – already accounts for volume taken by the sumps.

b. i_vertical - # of BiMAC pipes beyond which the pipes are subject to thermal load on the vertical part (at the center: # 1, at the far end: #51).

c. The total ESBWR vessel inventory is: 220 metric tons (240 tons) Fuel, 76 metric tons (84 tons) Zirconium, and 50 metric tons (55 tons) S-S. An oxidic pool would contain, besides the fraction of the fuel assumed, the fraction of Zr assumed to have oxidized (typically 30%, or 27 metric tons (30 tons)), some fraction of the steel inventory, and the amounts of refractory material assumed to have melted in.

d. The up-to-down power split was taken as 3:1, and side-fluxes, as per simulations, at ~300 kW/m^2 (26 $Btu/s.ft^2$).

Table 21.5.4.3-2

Computational Domain of Melt Pool Configuration I

Computational Domain of Melt Pool Configuration I
(Central Slice of the Wedge, without Vertical Section)

Case	A	B	C
Melt pool's total height, H [m] (in)	0.2 (8)	0.4 (16)	0.6 (24)
Horizontal span of the inclined boundary, L_C [m] (ft)	1.13 (3.71)	2.27 (7.45)	3.40 (11.2)
Height of vertical boundary, H_V [m]	0	0	0

Table 21.5.4.3-3

Computational Domain of Melt Pool Configuration II

Computational Domain of Melt Pool Configuration II,
(Near-Edge Slice of the Wedge, with a Vertical Section)

Case	M	N	O
Melt pool's total height, H [m] (in)	0.6 (24)	0.6 (24)	0.4 (16)
Horizontal span of the inclined boundary, L_C [m] (ft)	1.13 (3.71)	2.27 (7.45)	1.13 (3.71)
Height of vertical boundary, H_V [m] (in)	0.4 (16)	0.2 (8)	0.2 (8)

Table 21.5.4.3-4

Fluid Thermo-Physical Properties and Parameters Used

Properties and Parameters	Value
Density, ρ [kg/m^3] (lbm/ft^3)	8000 (500)
Thermal conductivity, k [W/m.K] (Btu/hr.ft.F)	4 (2.3)
Heat capacity, C_P [J/kg.K] (Btu/lbm.F)	300 (0.072)
Thermal diffusivity, α [m^2/s] (ft^2/s)	1.67×10^{-6} (1.80×10^{-5})
Thermal expansion coefficient, β [1/K] (1/F)	0.002 (0.001)
Viscosity, μ [Pa.s] (lbf.s/ft^2)	0.01 (2×10^{-4})
Prandtle Number $Pr = \nu/\alpha$	0.75
Heat generation rate, qVol [MW/m3] (Btu/hr.ft^3)	1 (97,000)
Angle of inclination, °	10

Table 21.5.4.3-5
Power Split and Peaking Factor Results

Summary of Power Split and Peaking Factor Results from the Direct Numerical Simulations [all fluxes in kW/m2 (Btu/s.ft^2)].

Case No.	q_{up}	q_{dn}	q_s	q_{up} / q_{dn}	q_{max} / $q_{dn\ or\ s}$
A	63 (5.5)	30 (2.6)	N/A	2.1	1.25
B	120 (10.5)	54 (4.8)	N/A	2.2	1.25
C	178 (15.7)	80 (7.0)	N/A	2.2	1.25
C-3D	238 (21.0)	68 (6.0)	N/A	3.5	1.2
M-3D	286 (25.2)	85 (7.5)	280 (24.7)	3.4	3.0 / 1.4
M	255 (22.5)	125 (11.0)	330 (29.1)	2.0	3.0 / 1.4
N	238 (21.0)	126 (11.1)	340 (29.9)	1.9	3.0 / 1.2
O	168 (14.8)	83 (7.3)	245 (21.6)	2.0	3.0 / 1.2

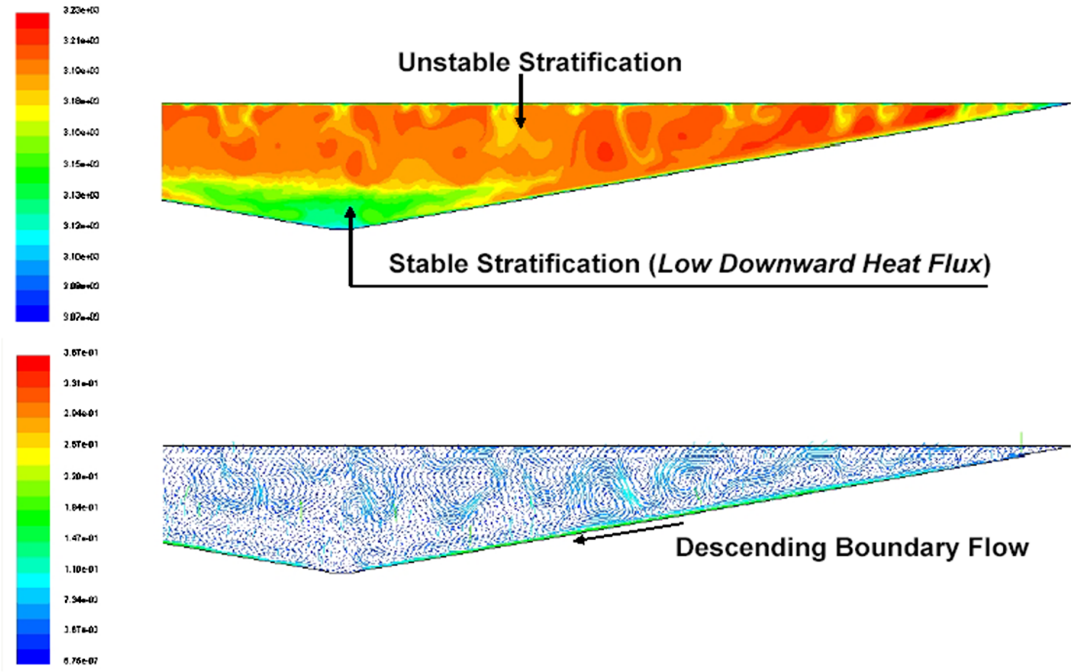

Figure 21.5.4.3-1a. Temperature and Velocity Fields in Configuration I (Case C)

Temperature (top) and velocity (bottom) fields in Configuration I (Case C).

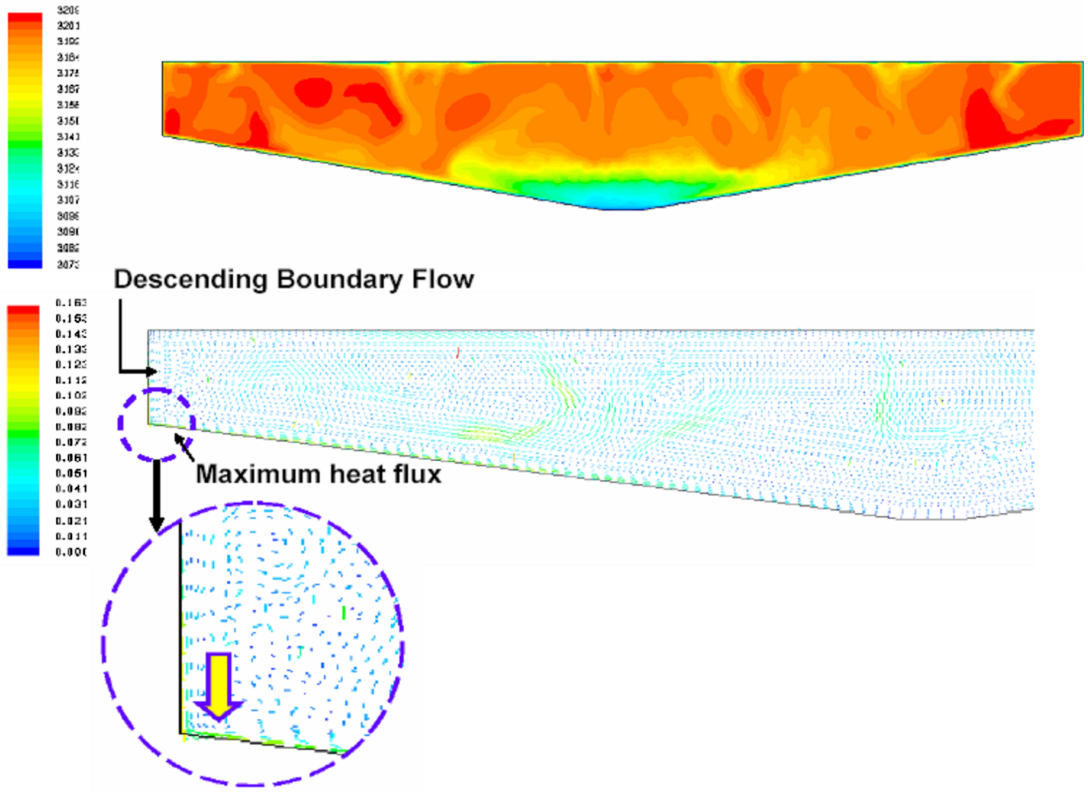

Figure 21.5.4.3-1b. Temperature and Velocity Fields
Temperature and velocity fields in Configuration II (Case O)
Temperature (top) and velocity (bottom) fields in Configuration II (Case O)

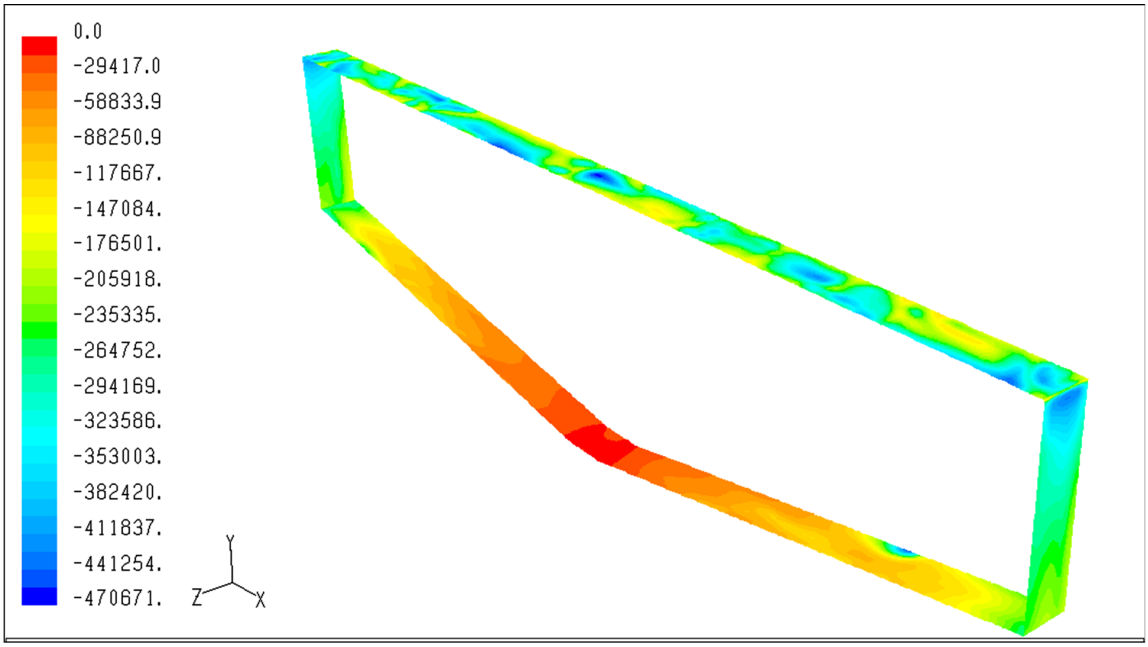

Figure 21.5.4.3-2. Heat Flux Map at Pool Boundaries for Configuration II

Instantaneous map of heat flux at the pool's boundaries from 3D simulation of Configuration II (Case M-3D) over a width of 0.2 m. Note the negative sign on the scale: the highest absolute heat flux is in dark blue, and the smallest is in red.

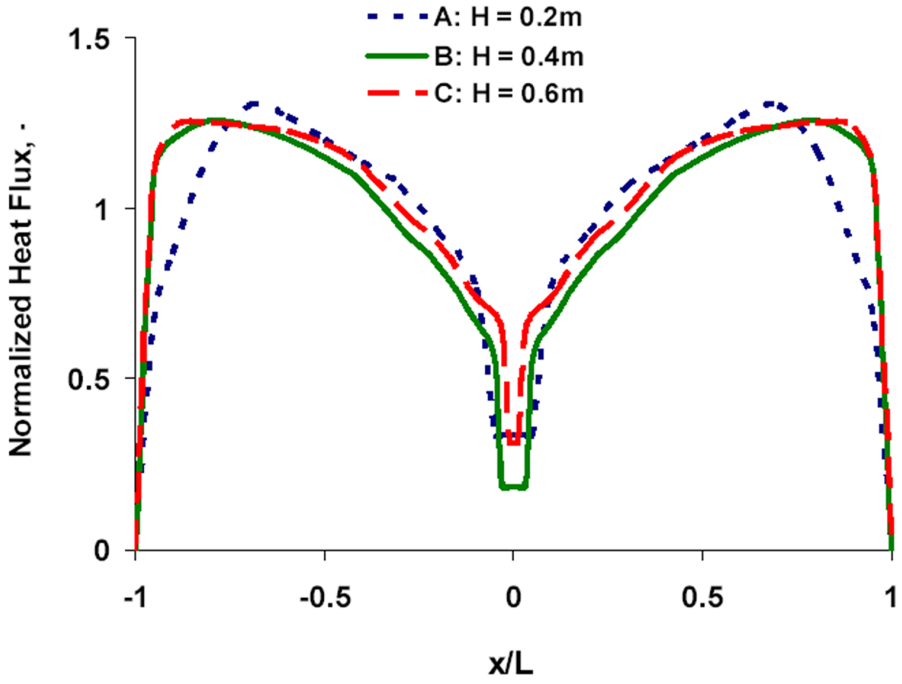

Figure 21.5.4.3-3. Configuration I Results

Downward heat flux distributions along the inclined boundary (total length L).

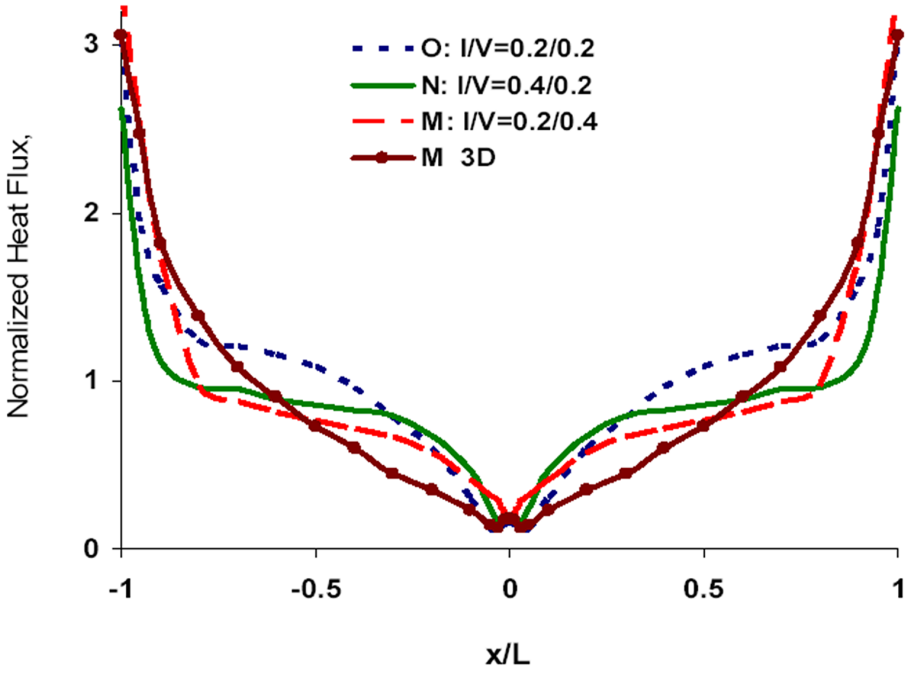

Figure 21.5.4.3-4. Configuration II Results

Downward heat flux distributions along the inclined boundary. (I/V denote pool dimensions of the "inclined/vertical" sections of the boundary respectively).

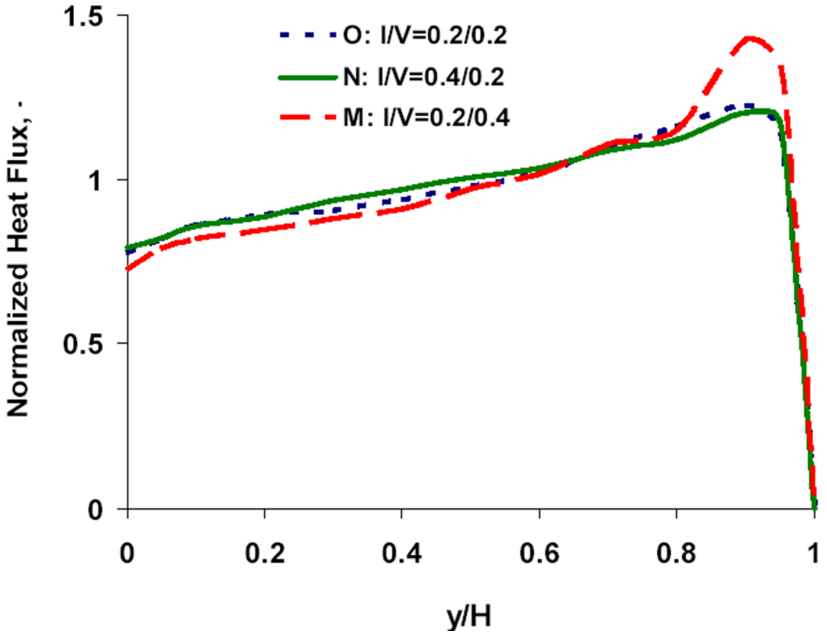

Figure 21.5.4.3-5. Configuration II Results

Sideward heat flux distributions along the vertical pool boundaries of length H. (I/V denote heights of the "inclined/vertical" sections of the pool boundaries respectively).

Protective Layer Ablation under Melt-Jet Impingement

Zirconia is known to be highly stable in oxidizing atmospheres, and inert in contact with most metals at high temperatures, including molten steels and zirconium, so no chemical ablation of the refractory layer is expected if the discharge happens to be metallic. For metallic melts no thermal (melting) ablation is possible either because Zirconia melts at a temperature range (of 2950 - 3120 K (4850 – 5160°F)) that is far above any conceivable metallic temperatures in the core debris. Thus we need only be concerned here with oxidic melts that are very highly superheated.

Pure oxidic materials, such as UO_2 or ZrO_2, have melting points of ~3,000 K (4900°F), which is close to the Zirconia melting range, however, as these oxides interact with other materials, including control rod materials during the formation of the melt pool in the lower plenum, eutectic mixtures are formed (Asmolov, 2000) and melting temperatures as low as 2340 K (3750°F) can be expected. Consequently, given a few 100's K of superheat at the time of vessel breech, the relevant melt temperatures to assess protective layer performance are in the ~2,600 K (4200°F) range, and still well below what is needed to effect melt attack on the Zirconia.

We emphasize that this logic is meant to apply only in the short-term, impingement process that would occur during the first, major relocation event. In the longer term, if the debris is not coolable from above, a combination of melt superheating and eutectics formation should yield ceramic ablation to the extent needed to conduct the needed amount of heat flux into the boiling of water flowing inside the BiMAC.

Further perspective on the question of ablation by an oxidic melt can be gained by calculating the ablation rate for an assumed pure oxidic melt at a temperature of 3,100 K (5100°F), which is a 100 K (180°F) superheat. We employ the Saito (1989) correlation, as it has been independently verified by additional experiments, and further established on theoretical grounds (Dinh et al, 1997).

$$Nu = 0.0027\ Re.Pr = 0.0027\ Pe = 0.0027\ U\ d/\alpha$$

Where U is the velocity, d is the jet diameter, and α is the thermal diffusivity, all referring to melt quantities. Thus the heat flux is found as,

$$q = \Delta T\ \ h = \ 0.0027\ U\ \rho\ C\ \Delta T$$

where ρ, C, and ΔT are the melt density, heat capacity, and superheat respectively. The ablation rate is then found by dividing this heat flux into the heat capacitance (including the heat of fusion) of the Zirconia (1,700 kJ/kg (730 Btu/lbm), and 6,100 kg/m^3 (380 lbm/ft^3)).

Applied this for a HP scenario with d= 0.2 m (8 in), ΔT= 100 K (180 °F), and U= 40 m/s (130 ft/s), we obtain a heat flux of ~26 MW/m^2 (2300 Btu/s.ft^2) which would give an ablation rate of 2.5 mm/s (0.098 in/s). Such a pour involving 120 metric tons (130 tons) would last for ~30 s, and would produce a total ablation of ~8 cm (3 in). For LP scenarios lower jet velocities would be exactly compensated by longer pour times, yielding the same result, unless the superheat was different. For example a superheat of 200K (360 °F), for the same-volume pour, would produce a total ablation depth of 16 cm (6 in).

21.5.4.4 Quantification of Fragility

Fragility of BiMAC is considered here according to the decomposition shown in Figure 21.5.4.2-1; namely, failure due to (short-term) interactions between melt and BiMAC pipes during melt relocation, and failure due to long-term thermal loading (melt pool convective heat transfer). The latter, in turn, consists of two aspects: (i) natural circulation flow stability as potentially impacting the development of dry-outs, and (ii) local heat fluxes exceeding the burnout heat flux.

a. Structural Failure Criteria for an Ablated Zirconia Layer. Noting that the protective layer is well supported from below, and that such a ceramic layer when well-cast and cured is very tough, especially to compression, we believe any macroscopic thickness remaining (after ablation) would be sufficient to protect the BiMAC pipes. We will take a thickness of 50 mm (2 in) to represent, conservatively, the failure threshold. [Final design details of the BiMAC will be consistent with Reference 21.5-40.]

b. Natural circulation of coolant flow in BiMAC. This failure mode is assessed by means of the two-phase flow model described in Appendix E. Of interest is to determine at what power level the natural circulation flow becomes susceptible to Ledineg instability, or in other words, at what power level the two-phase pressure drop causes a sufficient reduction in flow to yield a near-voided condition in the BiMAC channels. As shown in Appendix E, multi-channel flow demand on the BiMAC header can be satisfied by multiple down-comers, so that performance can be adequately matched by using a single channel for both the Downcomer and the Riser.

The basic trend in the results can be seen in Figures 21.5.4.4-1 and 21.5.4.4-2. They show flow rates and exit void fractions as functions of supplied heat flux. The latter is applied uniformly over the whole of the riser, which includes the inclined and the vertical portions of the boundary. The effect of non-uniform power supply was evaluated, within the limits that are reasonable in the BiMAC environment, and it was found to be negligible. We consider only a central channel, and saturated water at the inlet, which provide the most limiting conditions for present purposes.

In Figure 21.5.4.4-1 we note the broad maximum in flow rate obtained at heat fluxes around 100 kW/m^2 (8.8 Btu/s.ft^2), the value that represents an upper bound of what would be possible in the LDW of the ESBWR. The decline in flow rates is due to two-phase pressure drop compensating at an increasing rate for the increased gravity head created by an increased channel voiding condition. In Figure 21.5.4.4-2 we can see this increase in voiding with heat flux. The increase is monotonic, and reaches up to an exit void fraction of ~40% found for a heat flux level of 100 kW/m^2 (8.8 Btu/s.ft^2). The flow is stable throughout this range of possible conditions in that the rates of change of gravity head with increasing heat flux is higher than the change in demand due to increase in frictional pressure drop.

In regards to dryout due to water depletion, it is clear that a 40% exit void fraction would not place the channel at any such risk. In Figure 21.5.4.4-2 we show the 70% exit void fraction level as a potential demarcation of the water-deficient regime, and the figure further shows that the relevant heat flux level would then be ~350 kW/m^2 (31 Btu/s.ft^2) –it is emphasized that this is for an average heat flux applied to the whole length of the longest, central channels of the BiMAC. Much higher fluxes would be needed for the middle or near-edge channels that are shorter and have vertical sections.

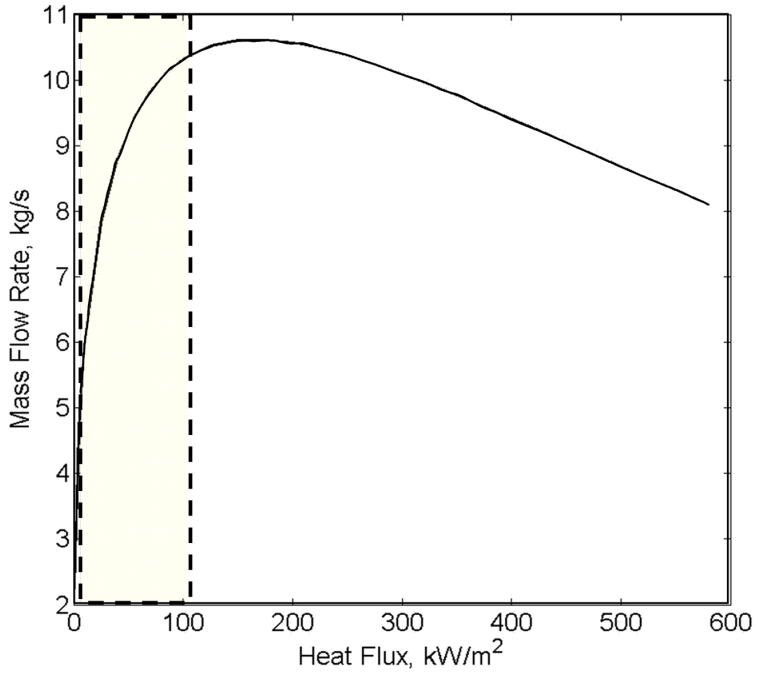

Figure 21.5.4.4-1. Mass Flow Rate Through a Bimac Channel

Predicted mass flow rate through a BiMAC channel, in natural convection, as function of applied heat flux (based on the pipe projected area). Shaded is the relevant range of heat fluxes.

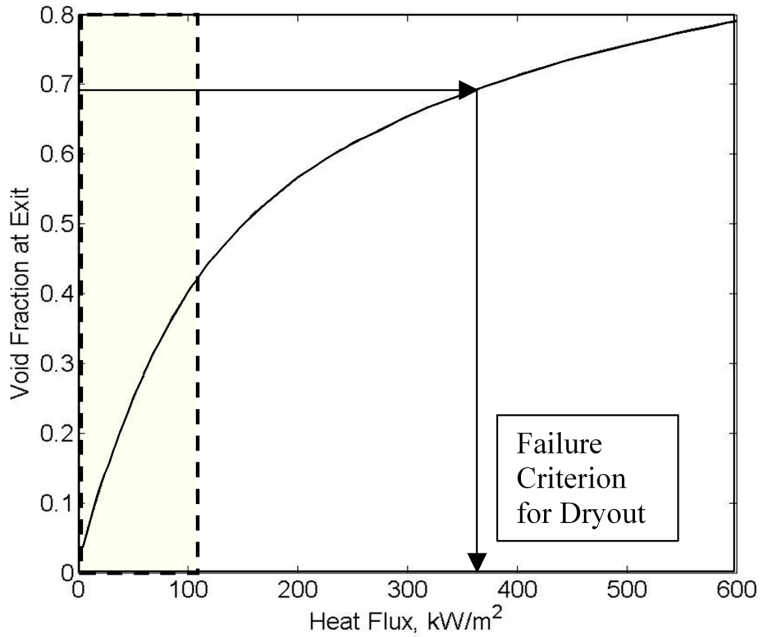

Figure 21.5.4.4-2. Void Fractions at the Exit of a Bimac Channel

Predicted void fractions at the exit of a BiMAC channel, in natural convection, as function of applied heat flux (based on the pipe projected area). Shaded is the relevant range of heat fluxes.

Quantification of fragility (Addendum of July 31, 2006)

Another perspective on the margins to failure due to this mechanism that can limit coolability can be gained by determining, in the fashion employed in Section 21.5.4.4 (b), the pipe diameter for which, at a heat flux level of 100 kW/m^2 (8.8 Btu/s.ft^2), the change in flow due to increase in power level first becomes negative. As can be seen from Figures 21.5.4.4.1a to 21.5.4.4.2b, this condition is bracketed between pipe diameters of 5 and 7.5 cm (2 and 3 in).

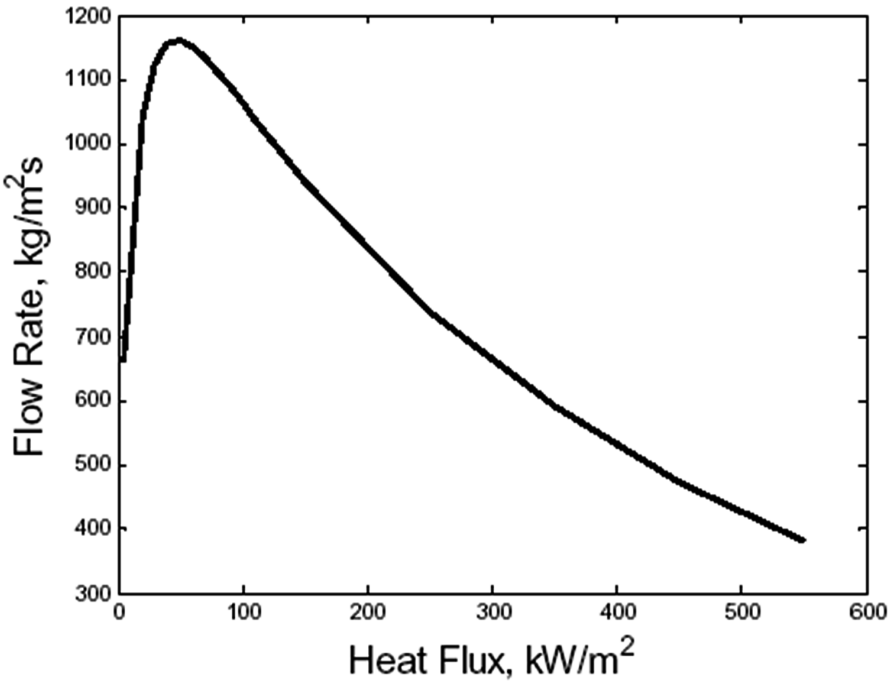

Figure 21.5.4.4.1a. Same as Figure 21.5.4.4-1 but with a pipe diameter of 5 cm.

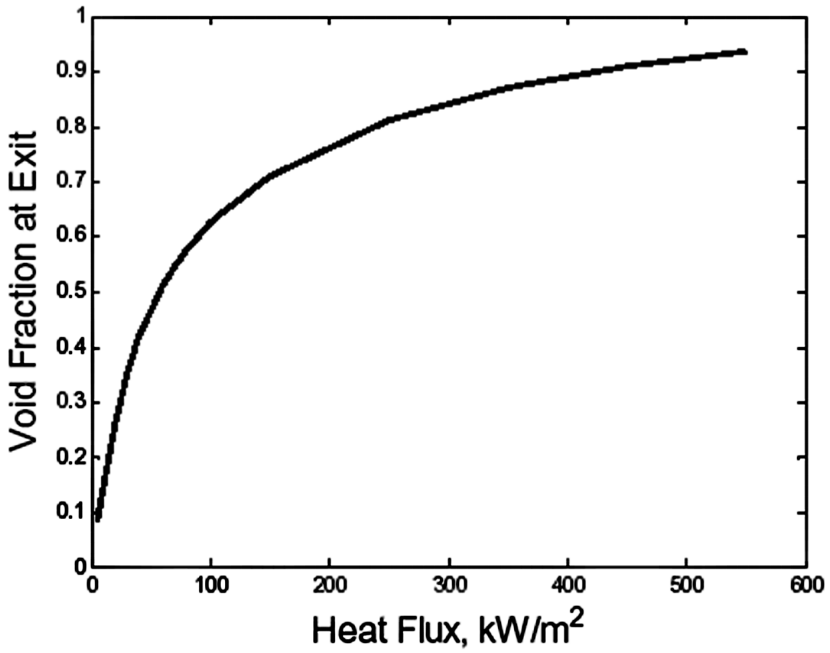

Figure 21.5.4.4.2a. Same as Figure 21.5.4.4-2 but with a pipe diameter of 5 cm

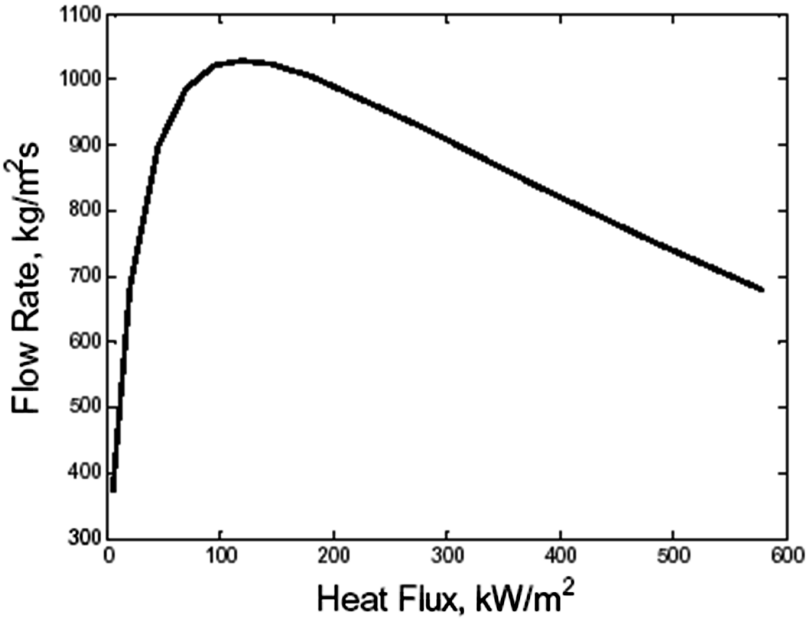

Figure 21.5.4.4.1b. Same as Figure 21.5.4.4-1 but with a pipe diameter of 7.5 cm.

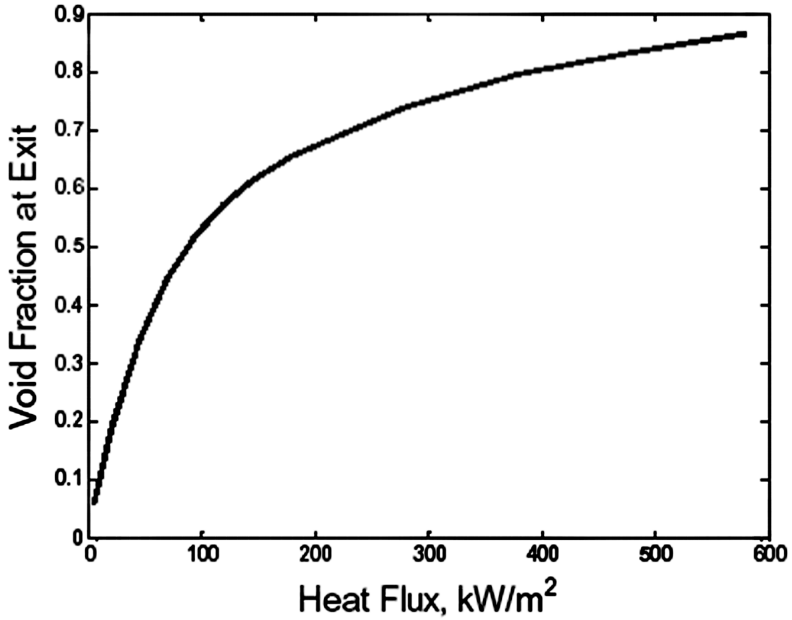

Figure 21.5.4.4-2b. Same as Figure 21.5.4.4-2 but with a pipe diameter of 7.5 cm

Limits to Coolability. For the pipes that make up the lower boundary of the BiMAC jacket we make use here of experiments made to support the IVR case for the AP600, and the Loviisa reactor in Finland (Theofanous et al 1996, 1994). These experiments were done in a series of several geometric configurations, and these evolved along the way as understanding was being developed. It turns out that the very first of the ULPU setups, the one known as Configuration I (C-I), were designed to address what at the time was the principal unknown, namely the inverted, near horizontal geometry at the pole of the lower head. It turns out that this design matches exactly the geometry of interest here (Figure 21.5.4.4.3). All the rest of the test program, performed over the period of some years, and spanning a total of five configurations, provides a further support of these first results, as well as of our effort to relate and interpret them for our purposes here. In particular, the emphasis in this program shifted with time to the more limiting (for the PWR IVR) near-vertical boundary, at the upper edge of the lower head. This is relevant here too, as it characterizes the Critical Heat Flux (CHF) on the pipes that make up the vertical boundary of the BiMAC. For this relevant is the ULPU Configuration IV (Figure 21.5.4.4-4). The pool boiling data from C-I is reproduced in Figure 21.5.4.4-5, and those from C-IV in 21.5.4.4-6. In both C-I and C-IV the channel cross section was 10x15 cm (3.9 x 5.9in), which is quite close to that of a BiMAC pipe.

In Figure 21.5.4.4-5 we can see that according to these data, and for the range of inclination angles θ of our interest ($\theta \sim$ 10-15°), the CHF is in the range of 450 to 550 kW/m^2 (40 to 48 Btu/s.ft^2). It should be noted that these test were conducted at pool boiling conditions (no net flow supplied) and rather low submergence, so we can expect they provide a conservative representation of BiMAC forced (initially) or natural (the rest of the time) convection environment.

In Figure 21.5.4.4-6 we can see that at near vertical orientation a CHF of 1 MW/m^2 (88 Btu/s.ft^2) is quite appropriate. Indeed, this estimate is robust as this would be also a typical lower bound of CHF from an upwards-facing flat plate (engineering surface) in water.

While as we see in the next section further enhancements are hardly needed, it may be worth pointing out that CHF enhancement technology has been advanced greatly over the past decade, and that we would plan to take advantage of them in the final design to be carried out at the COL stage. These advances are due to both improvements in basic understanding of high heat-flux boiling and burnout physics, as well as empirical development of innovative approaches, which make use of heater surface treatment and coolant chemistry to improve the coolability limit in boiling systems. In particular, we note that the C-I experiments were conducted with distilled water, whereas both reactor water and GDCS water are not distilled. In our recent work for the AP1000, we established a significant, beneficial effect of reactor (and containment) water chemistry on CHF (see Dinh, Tu and Theofanous, 2003; Tu, Dinh and Theofanous, 2003; Theofanous and Dinh, 2004).

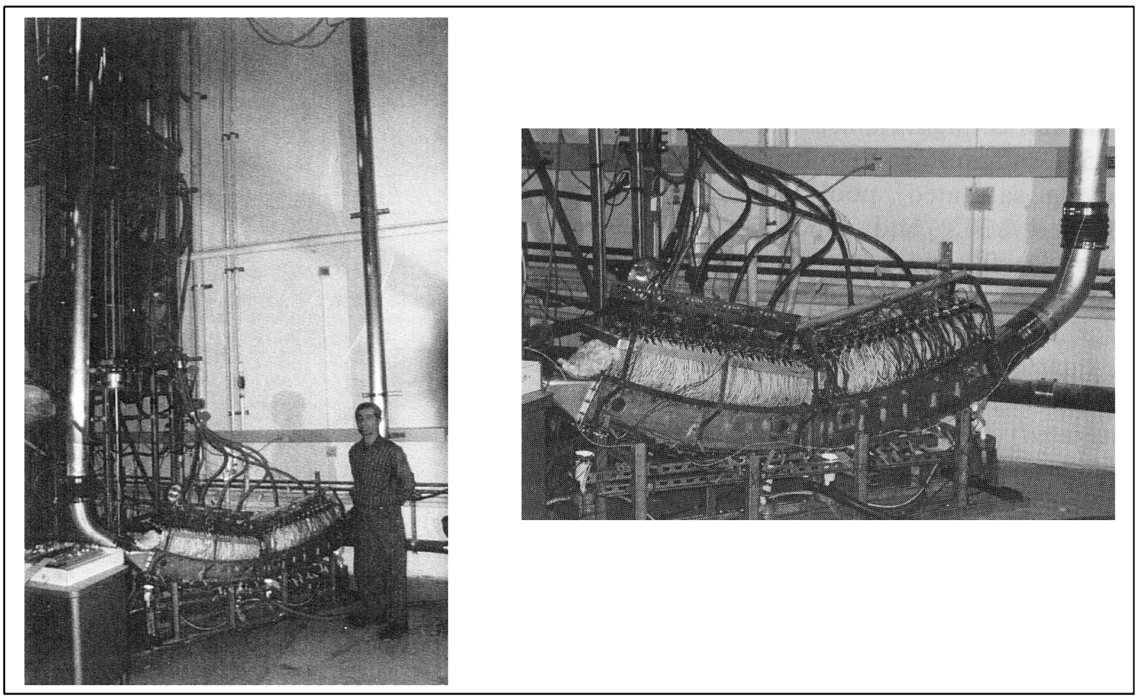

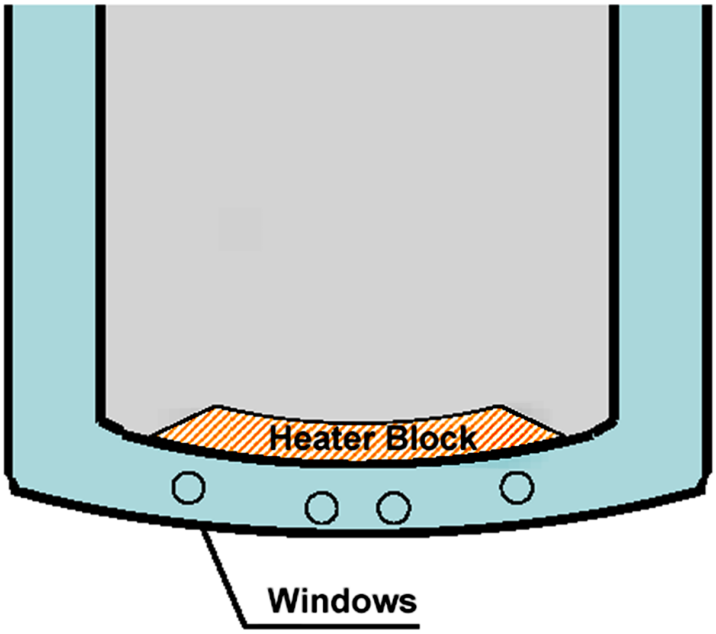

Figure 21.5.4.4-3. Pictures and Schematic of the Ulpu Configuration C-I

Pictures and schematic of the ULPU Configuration C-I: low-submergence, pool-boiling conditions. Similarity between C-I and BiMAC is rather straightforward.

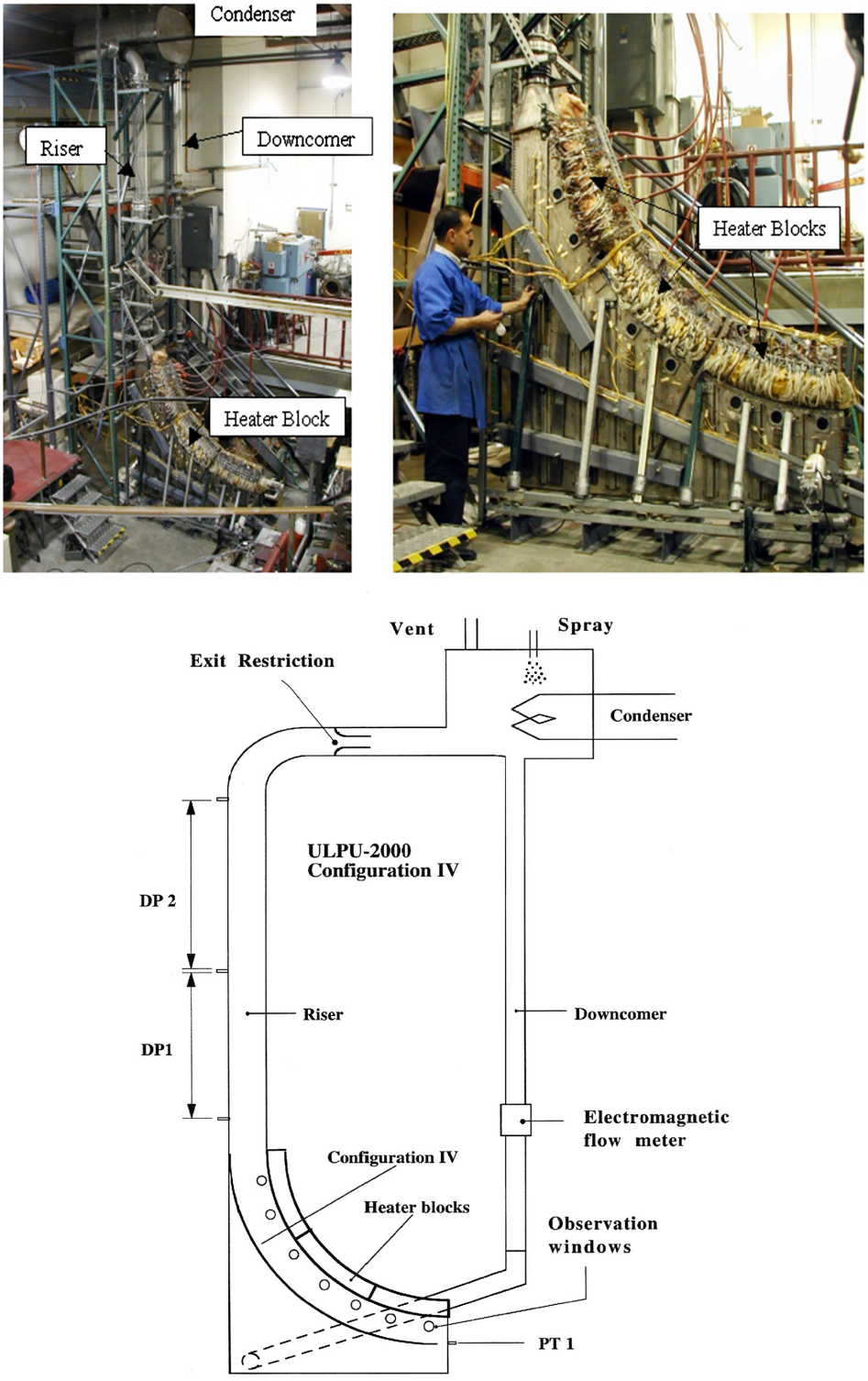

Figure 21.5.4.4-4. Pictures and Schematic of the ULPU Configuration C-IV

The ULPU Configuration C-IV. The curved baffle shown creates a channel similar to a BiMAC in regards to the vertical segment of pipe. The pool boiling condition is defined by a water level near the exit of the curved portion of the flow channel.

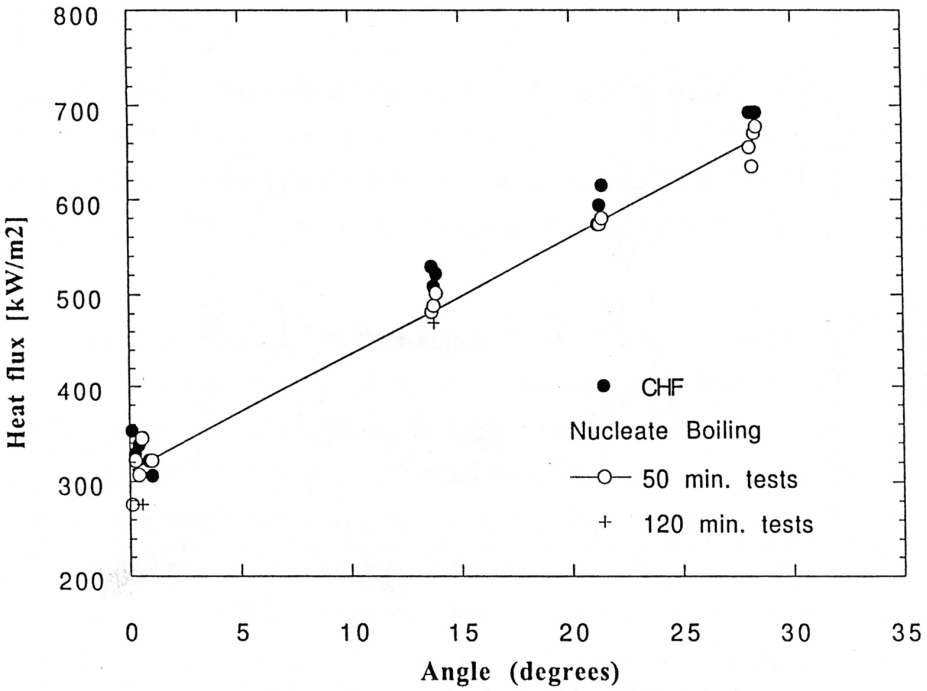

Figure 21.5.4.4-5. Critical Heat Flux Measured in ULPU C-I

Critical Heat Flux measured in ULPU C-I (near horizontal, inverted geometry) under pool boiling conditions (Theofanous et al., 1994b).

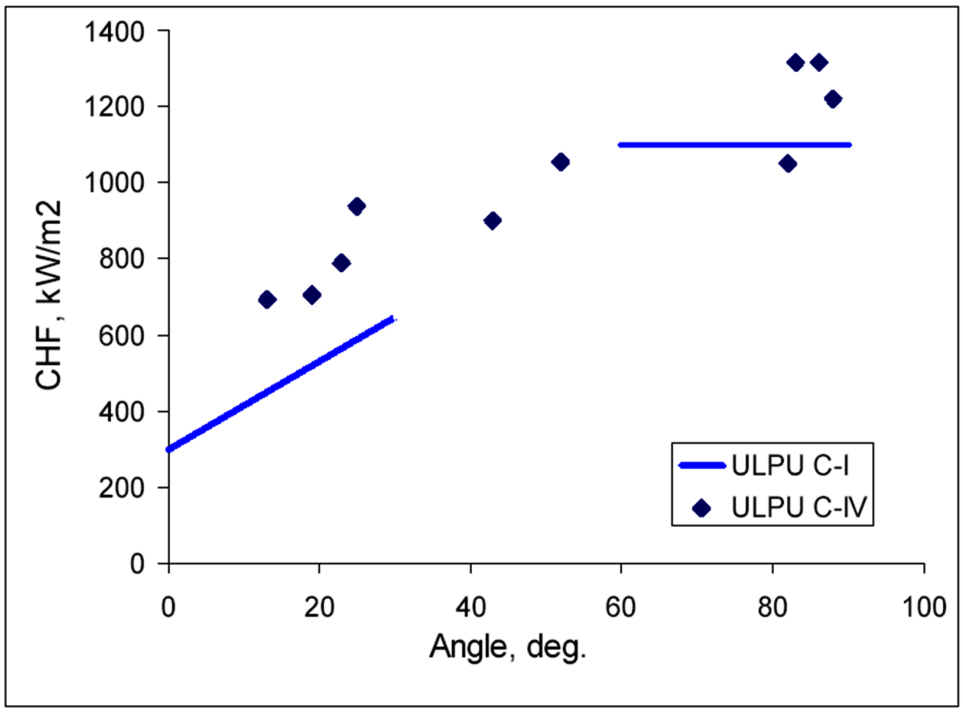

Figure 21.5.4.4-6. Critical Heat Flux Measured in ULPU C-IV

Under pool boiling conditions (Theofanous et al., 1994b; 1996).

21.5.4.5 Predication of Failure Probability

Combining the results of the previous two sections we can now evaluate the likelihood of BiMAC device's failure to function for its intended purpose as follows:

a. The ceramic-refractory material of the protective layer is only susceptible (by ablation) to superheated oxidic melt impingement. Even then it would require a melt a melt volume of ~500 metric tons (550 tons) to penetrate the 200 mm (8 in) layer down to within 50 mm (2 in) from the BiMAC pipes. Thus failure by melt impingement is physically unreasonable. [Final design details of the BiMAC will be consistent with Reference 21.5-40.]

b. For the range of thermal loadings that are applicable to non-coolable melt-pool configurations in the LDW, two-phase natural circulation is seen to be quite sufficient in supplying the BiMAC pipes with a cooling stream that is stable, and of sufficiently high liquid (water) content to ensure a well-wetting condition very where. As shown in Figure 21.5.4.5-2, the available margin is over 300%. Thus, failure by dry-outs due to flow and water supply deficiencies is physically unreasonable.

c. As indicated in Figures 21.5.4.5-1 and 21.5.4.5-2, the (conservatively estimated) margins to local burnout are anywhere from 500% for a central channel, to 100% near the top of a vertical channel, to 60% near the edges of the inclined lower boundary of a near-edge channel. These margins, placed on the basis of bounding estimates both for thermal loads and burnout heat fluxes, dwarf any uncertainties due to the small geometric differences between BiMAC pipes and the ULPU test sections. Thus, failure due to local burnout is physically unreasonable.

d. Finally we note that the BiMAC cooling jacket protects also the two sumps found in the LDW floor in a way that prevents melt from entering them. [The Drywell LCW Sump will be located above the lower drywell floor.]

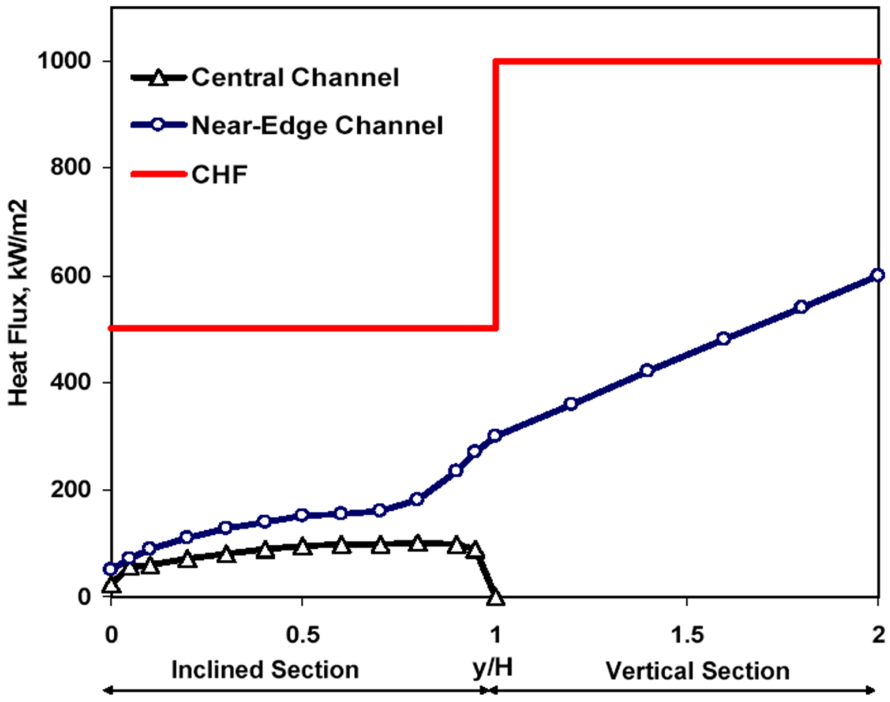

Figure 21.5.4.5-1. Local Thermal Loads and Coolability Limits in BiMac

Local thermal loads and coolability limits in BiMAC at bounding conditions and estimations.

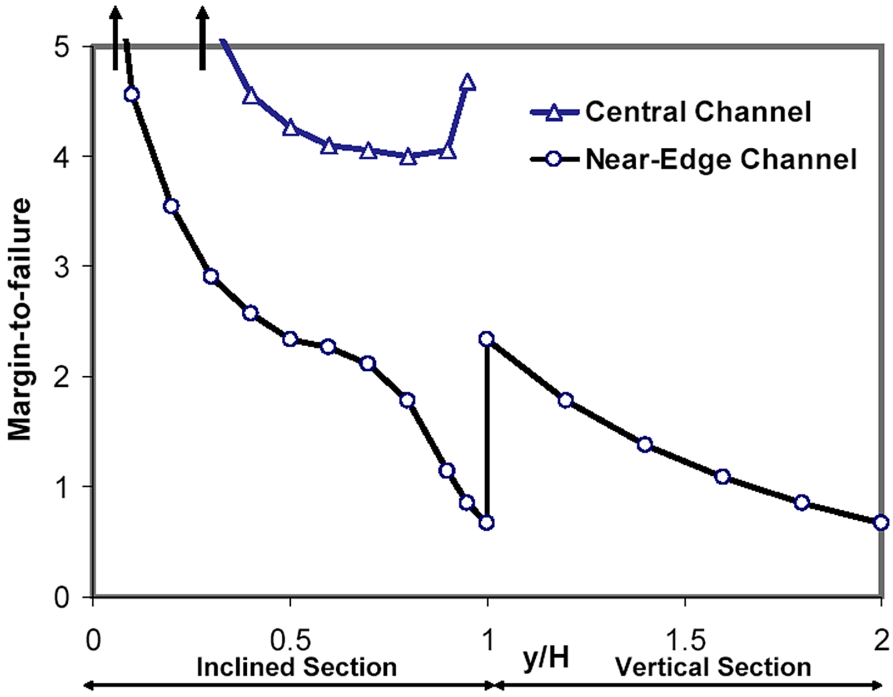

Figure 21.5.4.5-2. Margins to Burnout in BiMAC

The margin to burnout in BiMAC is defined as (qCHF/q – 1) where q is the local bounding heat flux, and qCHF is the local minimum bound of burnout flux.

21.5.5 Summary and Conclusions for BMP

We have shown that the BiMAC device is effective in containing all potential core melt releases from the RPV in a manner that assures long term coolability and stabilization of the resulting debris. In this way the concrete basemat penetration issue becomes mute, and so is containment over-pressurization by concrete decomposition gases.

The principal ingredients in this effective functioning of the device can be recapitulated as follows:

a. Choice of a refractory ceramic material as a protective layer, that eliminates ablation by superheated metallic jets, and a layer thickness chosen so as to provide ample margins to the ablation front reaching the BiMAC pipes even under the most extreme, large-volume-pours of superheated melts (for both for LP and HP scenarios);

b. Positioning and dimensioning of the cooling jacket (the BiMAC pipes) so that while resistant to significant dynamic loads (see Section 21.4), they allow for stable, low-pressure-loss, natural circulation that is not susceptible to local burnout due to thermal loads exceeding the critical heat flux, or to dry-outs due to flow and water deficient regimes;

c. Sizing and positioning the BiMAC in the LDW in such a way that all melt released from the vessel is captured (except of course of any melt dispersed to the UDW in HP scenarios) and contained within, and;

d. Providing for an angle of inclination of the lower boundary that balances the various requirements, including operational space available, and good margins to local burnout.

Summary and Conclusions for BMP (Addendum of July 31, 2006)

In addition to the thermal load considerations detailed in this chapter, and the upcoming BiMAC experiments, the detailed design of BiMAC will involve considerations of external protection against mechanical loads, such as may be generated by falling, or ejected objects/debris following RPV failure. This addendum is to note that this design effort will be facilitated by relaxing the melt-retentive property originally envisioned for the BiMAC cover plate, and now found to be unnecessary.

In particular, rather than requiring that this cover plate be readily penetrable by impinging molten core material, we now prefer that it be materially substantial, thermally robust, and it be well supported from below in a manner that offers a naturally protective function.

In considering potential mechanical loads for the detailed design, we recognize that:

a) Because in the ESBWR design the control rod drives (CRDs) are “hooked” to the lower core support plate, they cannot fall even if the welds that seal the lower head penetrations were to melt out (actually this hooking is to protect against rod ejection in case of such a failure under normal operation). Thus the only mechanism for failure is detachment of one or more instrument tubes. While not supported externally in a manner that would prevent their total detachment, these tubes have restraints that would impede their motion following such detachment, and these would have to be taken into account in defining the design criteria for the BiMAC cover plate. In addition this would have to include the protective function of the intervening CRD-maintenance platform.

b) Because the CRD motors along with related supports form a massive and compact region at the lower ends of the CRDs, any jet(s) emanating from instrument tube penetration failures on the lower head would be disrupted and dispersed. This dissipation/defocusing of mechanical as well as thermal energy loads beneficially impacts the design requirements for protection of the BiMAC, including its ceramic sacrificial layer.

c) This enhanced protection is consistent and of benefit in the reliability design of the BiMAC flooding deluge system, as it relaxes the timing requirements for activation, following the instant of initial RPV failure and melt release. Of further benefit in this regard is the appreciation that the initial release would be metallic and of rather limited quantity.

Further comments on mechanical loads (Addendum of May 7, 2007)

This is written in response to Dr. Henry's suggestion for a more detailed consideration of the physics involved (along a ROAAM framework) in mechanically loading the BiMAC due to detachment of lower head penetrating structures. While initially this was our intent too, further considerations of the coolability limits of BiMAC, such as those provided by Drs. H. Fauske and M. Fisher during the review process, suggest margins to failure that may allow a much lower angle of inclination of the BiMAC pipes. This, in addition to other considerations on thermal aspects, suggest that the final detailed design could be made to incorporate such large amounts of sacrificial material as to make the issue of mechanical impacts mute. Thus we would rather wait for the BiMAC coolability results before we finalize design in a manner consistent, and to the extent possible optimal in every respect including mechanical loads of the type raised in this review.

21.5.6 Add BiMAC Testing (Addendum of September 25, 2007)

Testing of the BiMAC design was completed and final design parameter selection has been made. The results indicate that the BiMAC performance meets performance objectives with ample margins. Documentation is provided in NEDE-33392P; "The MAC Experiments: Fine-tuning of the BiMAC Design", Proprietary Report by T.G. Theofanous. Reference 21.5.-40.

21.5.7 References

21.5 -1 S. Angelini, Y. Buyevich and T.G. Theofanous, "The Mechanism and Prediction of Critical Heat Flux in Inverted Geometries," NURETH-8, Kyoto Japan, September 30-October 4, 1997, Vol. 1, 147-156.

21.5-2 Asmolov, V.V. (2000), "RASPLAV Project Major Activities and Results," RASPLAV Seminar, Program Review Meeting of OECD RASPLAV Project, November, 2000, Munich, Germany.

21.5-3 Asmolov, V.V., S.S. Abalin, A.V. Merzliakov, V.N. Zagryazkin, Ye.V. Astakhova, I.D. Daragan, V.D. Daragan, Ye.K. D'yakov, A.Yu. Kotov, A.S. Maskaev, Ye.M. Rakitskaja, V.M. Repnikov, V.Yu. Vishnevsky, V.V. Volko; A.G. Popkov, V.F. Strizhov, (2000) "RASPLAV Final report: Properties Studies: Methodology and Results." Kurchatov Institute, Moscow, 2000.

21.5-4 Dinh, T.N., and Nourgaliev, R.R. (1997). "Turbulence Modeling in Large Volumetrically Heated Liquid Pools," Nuclear Engineering and Design, 169, 131-150, 1997.

21.5-5 R.R. Nourgaliev, and T.N. Dinh, (1997). "The Investigation of Turbulence Characteristics in an Internally Heated Unstably Stratified Fluid Layers," Nuclear Engineering and Design, 178:(1), 235-259, 1997.

21.5-6 R.R. Nourgaliev, T.N. Dinh, and B.R. Sehgal, (1997a). "Simulation and Analysis of Transient Cooldown Natural Convection Experiments," International Journal of Nuclear Engineering and Design, 178:(1), pp.13-27, 1997a.

21.5-7 R.R. Nourgaliev, T.N. Dinh, and B.R. Sehgal, (1997b). "Effect of Fluid Prandtl Number on Heat Transfer Characteristics in Internally Heated Liquid Pools with Raleigh Numbers up to 1012," Nuclear Engineering and Design, 169, 165-184, 1997b.

21.5-8 Dinh, T.N., and Theofanous, T.G, (2003). "Nucleation Phenomena in Boiling," Multiphase Science and Technology. 15(1-4), pp.349-363, 2003.

21.5-9 Dinh, T.N., Tu, J.P., Salmassi, T., Theofanous, T.G, (2003). "Limits of Coolability in AP1000-Related ULPU-2400 Configuration V Facility," International Topical Meeting on Nuclear Reactor Thermal Hydraulics, Seoul, Korea, Oct., 2003.

21.5-10 Dinh, T.N., Tu, J.P. and Theofanous, T.G. (2004) "Hydrodynamic and Physico-Chemical Nature of Burnout in Pool Boiling," International Conference on Multiphase Flow, Yokohama, Japan, May 2004. Paper 296. 14p.

21.5-11 Dinh, T.N., Yang, Y.Z., Tu, J.P., Nourgaliev, R.R., and Theofanous, T.G. (2004a), "Rayleigh-Bénard Natural Convection Heat Transfer: Pattern Formation, Complexity and Predictability," 2004 International Congress on Advances in Nuclear Power Plants, Pittsburgh, PA, June 13-17, 2004.

21.5-12 T.N. Dinh, J.P. Tu, Y.Z. Yang, R.R. Nourgaliev and T.G. Theofanous (2004b), "Characterization and Predictability of Transient Heat Transfer in an Unstably

Stratified Layer during Power Startup," 37th AIAA Thermophysics Conference, Portland, OR, June 27-30, 2004. AIAA-2004-2733.

21.5-13 Fischer, M., (2003). "Severe Accident Mitigation and Core Melt Retention in the European Pressurized Reactor (EPR)," 11th International Conference on Nuclear Engineering, Tokyo, JAPAN, April 20-23, 2003, ICONE11-36196.

21.5-14 Fluent (2004). Fluent 6.0 -- CFD Code Manual.

21.5-15 Garching (1998) OECD/CSNI/NEA Workshop on "In-vessel core debris retention and coolability," Garching, Germany, 3-6 March, 1998.

21.5-16 GE-NE (2005a), ESBWR Certification Probabilistic Safety Assessment. NEDC-33201P. August 2005.

21.5-17 GE-NE (2005b), ESBWR Design Control Document. 26A6642BZ Rev.00. August 2005.

21.5-18 Grenoble (1994) OECD/CSNI/NEA Workshop on Large Molten Pool Heat Transfer, Nuclear Research Centre, Grenoble, France, March 9-11, 1994.

21.5-19 Kukhtevich, I.V., Bezlepkin, V.V, Leontiev, Yu. G., Strizhov, V., Proklov, V.B. (2001). "Severe Accident Management Measures for Tianwan NPP with VVER-1000," in "Implementation of Severe Accident Management Measures," Workshop Proceedings PSI-Villigen, Switzerland, 10-13 September 2001. Nuclear Safety NEA/CSNI/R(2001)20.

21.5-20 PSI Report Nr. 01-15, November 2001.

21.5-21 Kymäläinen, O., Tuomisto, H., Hongisto, O., and Theofanous, T.G. (1994). "Heat Flux Distribution from a Volumetrically Heated Pool with High Rayleigh Number," Nuclear Engineering & Design, 149, 401-408, 1994.

21.5-22 Kymäläinen, O., Tuomisto, H., and Theofanous, T.G. (1997). "In-vessel Retention of Corium at the Loviisa Plant," Nuclear Engineering & Design, 169, pp109–130, 1997.

21.5-23 Saito M., et al (1989), "Melting Attack of Solid Plate by a High-Temperature Liquid Jet- of Crust Formation," Nuclear Engineering & Design, 121, p.11, 1990.

21.5-24 Scobel, J.H., Theofanous T.G., and Conway, L.E. (2002). "In-Vessel Retention of Molten Core Debris in the Westinghouse AP1000 Advanced Passive PWR," Proceedings, ANS 2002 Annual Meeting, International Congress on Advanced Nuclear Power Plants.

21.5-25 ICAAP), Hollywood, FL, June 9-13, 2002.

21.5-26 Theofanous, T.G., Liu, C., Angelini, S., Kymäläinen, O., Tuomisto, H., and Additon, S., (1994a). "Experience From the First Two Integrated Approaches to In-Vessel Retention Through External Cooling," OECD/CSNI/NEA Workshop on Large Molten Pool Heat Transfer, Nuclear Research Centre, Grenoble, France, March 9-11, 1994.

21.5-27 Theofanous, T.G., Syri, S., Salmassi, T., Kymäläinen, O. and Tuomisto, H. (1994b). "Critical Heat Flux Through Curved, Downward Facing, Thick Walls," Nuclear Engineering & Design, 151, 247-258, 1994.

21.5-28 Theofanous, T.G., Syri, S., Salmassi, T., Kymäläinen, O. and Tuomisto, H (1994c). "Critical Heat Flux Through Curved, Downward Facing, Thick Walls," OECD/CSNI/NEA Workshop on Large Molten Pool Heat Transfer, Nuclear Research Centre, Grenoble, France, March, 9–11, 1994.

21.5-29 Theofanous, T.G., Liu, C., Additon, S., Angelini, S., Kymalainen O., and Salmassi, T. (1996), "In-Vessel Coolability and Retention of a Core Melt," DOE/ID-10460, Vols. 1 and 2, October 1996.

21.5-30 Theofanous, T.G., Liu, C., Additon, S., Angelini, S., Kymalainen O., and Salmassi, T. (1997) "In-Vessel Coolability and Retention of a Core Melt," Nuclear Engineering & Design, 169 (1997) 1–48.

21.5-31 Theofanous T.G., and Syri, S. (1997) "The Coolability Limits of a Reactor Pressure Vessel Lower Head," Nuclear Engineering & Design 169 (1997) 59–76.

21.5-32 Theofanous T. G., Tu J. P., Maenpaa, T. K. (1998) "The Mechanism and Prediction of Critical Heat Flux in Inverted Geometries," Third International Conference on Multiphase Flow, Lyon, France, June 8-12, 1998.

21.5-33 Theofanous, T. G. and Angelini, S. (2000). "Natural Convection for In-Vessel Retention at Prototypic Rayleigh Numbers," Nuclear Engineering and Design, 200, 1-9, 2000.

21.5-34 Theofanous, T.G., Tu, J.P., Dinh, A.T. and Dinh, T.N. (2002a). "The Boiling Crisis Phenomenon. Part I: Nucleation and Nucleate Boiling Heat Transfer," Experimental Thermal and Fluid Science, 26, 775-792, 2002.

21.5-35 Theofanous, T.G., Tu, J.P., Dinh, A.T. and Dinh, T.N. (2002b). "The Boiling Crisis Phenomenon. Part II: Dryout Dynamics and Burnout," Experimental Thermal and Fluid Science 26, 793-810, 2002.

21.5-36 Theofanous, T.G. and Dinh, T.N. (2003), "On the Prediction of Flow Patterns as a Principal Scientific Issue in Multifluid Flow," Multiphase Science and Technology. 15(1-4), pp.57-76, 2003.

21.5-37 Theofanous, T.G. and Dinh, T.N. (2004), "High Heat Flux Boiling and Burnout as Microphysical Phenomena: Mounting Evidence and Opportunities," accepted for Multiphase Science and Technology. 2005. Also Keynote Paper. Japan-US Seminar on Two-Phase Flow Dynamics. December 6-11, 2004. Nagahama. CD-ROM Proceedings.

21.5-38 Theofanous, T.G. and Dinh, T.N. (2005) "Basemat-Internal Melt Arrest and Coolability (BiMAC) device." Patent Application. TcI/GE Document. GE Nuclear Energy. San Jose, March 30, 2005.

21.5-39 Tu, J.P., Dinh, T.N., Theofanous, T.G. (2003). "Enhancing Resistance to Burnout via Coolant Chemistry," 10th International Topical Meeting on Nuclear Reactor Thermal Hydraulics, Seoul, Korea, Oct., 2003.

21.5-40 The MAC Experiments: Fine-tuning of the BiMAC Design, Proprietary Report by T. G. Theofanous, NEDE-33392P.